*sustainability*

MDPI

*Article*

# Enhancing $CO_2$ Sequestration Through Corn Stalk Biochar-Enhanced Mortar: A Synergistic Approach with Algal Growth for Carbon Capture Applications

**Suthatip Sinyoung [1], Ananya Jeeraro [1], Patchimaporn Udomkun [2,3], Kittipong Kunchariyakun [4,5], Margaret Graham [6] and Puangrat Kaewlom [2,*]**

[1] Department of Civil and Environmental Engineering, Prince of Songkla University, Songkhla 90110, Thailand; ssuthatip@eng.psu.ac.th or suthattip.sin@gmail.com (S.S.); ananya.jeeraro8942@gmail.com (A.J.)
[2] Department of Environmental Engineering, Faculty of Engineering, Chiang Mai University, Chiang Mai 50200, Thailand; udomkun.patchimaporn@gmail.com
[3] Office of Research Administration, Chiang Mai University, Chiang Mai 50200, Thailand
[4] School of Engineering and Technology, Walailak University, Nakhonsithammarat 80160, Thailand; kunchariyakun.k@gmail.com or kittipong.ku@wu.ac.th
[5] Center of Excellence in Sustainable Disaster Management, Walailak University, Nakhonsithammarat 80161, Thailand
[6] School of GeoSciences, University of Edinburgh, Edinburgh EH9 3FF, UK; margaret.graham@ed.ac.uk
* Correspondence: kpuangrat@gmail.com or puangrat.k@cmu.ac.th

**Abstract:** This study examines corn stalk biochar (CSB)-enhanced mortar as an innovative material for carbon capture and $CO_2$ sequestration. CSB, a renewable agricultural byproduct, was incorporated into cement mortar at varying concentrations (2.5% to 75%), and its effects on the mortar's physicochemical properties, its ability to support algal growth, and the $CO_2$ absorption capacity of the algae were analyzed. Characterization of CSB showed a high carbon content (62.3%), significant porosity, and a large surface area (680.3 $m^2$ $g^{-1}$), making it ideal for gas capture. At low concentrations (2.5%), CSB slightly improved the mortar's compressive strength and density. However, higher CSB levels (5% to 75%) led to significant reductions ($p < 0.05$) in strength and density, while water absorption increased. $CO_2$ sequestration monitored from algal growth studies revealed that both *Chlorella* sp. (TISTR 8262) and *Scenedesmus* sp. (TISTR 9384) thrived on CSB-enhanced mortars. At a 75% CSB concentration, *Scenedesmus* sp. achieved a 24.2-fold increase in biomass by day 12, outperforming *Chlorella* sp., which showed a 26.6-fold increase. $CO_2$ absorption also improved with biochar. Mortars with 75% CSB achieved an 86% $CO_2$ absorption ratio without algae, while adding algae boosted this to nearly 100%, highlighting the synergistic effect of biochar and algal photosynthesis. Higher CSB levels accelerated $CO_2$ absorption stabilization, reaching saturation by day 8 at 75% CSB. *Scenedesmus* sp. showed slightly higher $CO_2$ absorption efficiency than *Chlorella* sp., reaching peak absorption earlier and maintaining greater efficiency. Higher CSB concentrations accelerated $CO_2$ absorption, indicating that biochar–mortar mixtures, particularly when combined with algae, provide a promising solution for enhancing carbon capture and sequestration in green infrastructure.

**Keywords:** microalgae cultivation; biochar-amended growth media; mortar and biochar synergy; sustainable algal biomass; green building materials; environmental remediation

check for updates

Academic Editor: Md. Shahinoor Islam

Received: 16 December 2024
Revised: 2 January 2025
Accepted: 3 January 2025
Published: 5 January 2025

**Citation:** Sinyoung, S.; Jeeraro, A.; Udomkun, P.; Kunchariyakun, K.; Graham, M.; Kaewlom, P. Enhancing $CO_2$ Sequestration Through Corn Stalk Biochar-Enhanced Mortar: A Synergistic Approach with Algal Growth for Carbon Capture Applications. *Sustainability* **2025**, *17*, 342. https://doi.org/10.3390/su17010342

**Copyright:** © 2025 by the authors. Licensee MDPI, Basel, Switzerland. This article is an open access article distributed under the terms and conditions of the Creative Commons Attribution (CC BY) license (https://creativecommons.org/licenses/by/4.0/).

## 1. Introduction

Global warming, driven by the anthropogenic emission of greenhouse gases (GHGs) such as carbon dioxide ($CO_2$), methane ($CH_4$), and nitrous oxide ($N_2O$), has emerged as

one of the most critical environmental challenges of our time. Among these gases, $CO_2$ is recognized as the principal contributor to global warming due to its high atmospheric concentration and long-term persistence [1]. Projections from the Intergovernmental Panel on Climate Change (IPCC) suggest that global temperatures could rise by 1.0 to 3.7 °C over the twenty-first century, depending on future GHG emission trajectories [2]. The ramifications of climate change are already visible, with increased frequency and severity of extreme weather events, rising sea levels, and significant disruptions to ecosystems and human health [3,4]. These alarming trends have spurred a global effort to reduce GHG emissions and enhance carbon sequestration to mitigate the effects of climate change.

One of the most promising strategies for mitigating $CO_2$ emissions is biological carbon sequestration, which captures and stores atmospheric $CO_2$ through natural processes. In recent years, biochar has emerged as a sustainable tool in this effort. Biochar is produced through the pyrolysis of biomass under oxygen-limited conditions at moderate temperatures, typically below 700 °C [5,6]. Its highly porous structure and large surface area make biochar particularly effective for improving soil fertility, enhancing microbial activity, and serving as a long-term carbon sink [7–10]. Given its ability to sequester $CO_2$ equivalents in terrestrial ecosystems, biochar is increasingly regarded as an eco-friendly material with substantial potential for climate change mitigation [11–14].

While the agricultural benefits of biochar are well documented, its application in other sectors, such as construction, has gained attention in recent years. Researchers have begun exploring biochar's integration into cement-based materials as a strategy to reduce the carbon footprint of the construction industry, which is responsible for a significant portion of global $CO_2$ emissions [15,16]. The global production of cement exceeds 4.1 billion tons annually, making it one of the largest contributors to industrial $CO_2$ emissions [16]. As concrete remains a cornerstone of modern infrastructure, finding innovative ways to incorporate environmentally friendly materials like biochar into cement formulations is crucial for reducing GHG emissions while maintaining material strength and durability [17,18].

Despite growing interest in biochar-enhanced cement mortar for its $CO_2$ absorption capabilities and improved mechanical properties [19,20], no studies to date have explored its potential as a medium for algae cultivation. This novel approach not only leverages biochar's material properties but also integrates biological carbon sequestration through algae cultivation, providing a dual-purpose solution for climate change mitigation. The scientific novelty of this study lies in the synergistic use of biochar-enhanced cement mortar as both a structural material and a biological growth medium for algae. This integration offers dual benefits: improved material properties and enhanced carbon capture through algae photosynthesis. Cultivating algae in such materials presents a unique opportunity to enhance carbon sequestration—algae are highly efficient at capturing $CO_2$ through photosynthesis, helping to reduce $CO_2$ levels in the atmosphere. While research in the construction industry has typically focused on preventing algae growth due to concerns over structural degradation and aesthetic damage [21,22], this study explores the innovative use of biochar in cement mortar to actively support algal growth rather than inhibit it. Although previous studies have examined algae cultivation for biochar production [23,24], little research has been conducted on using biochar as a supplement to growth media for algae [25].

This study presents a novel approach by investigating biochar-enhanced mortar as a platform for cultivating algae, specifically *Chlorella* and *Scenedesmus* species. These microalgae are not only efficient at $CO_2$ capture but also hold significant potential for bioenergy production [26–28], making them ideal candidates for integration with biochar-based materials. By aligning with several Sustainable Development Goals (SDGs)—such

as SDG 13 (Climate Action) and SDG 11 (Sustainable Cities and Communities)—this research contributes to the development of green infrastructure solutions that address global environmental challenges.

The primary objective of this research is to investigate the synergistic potential of biochar-enhanced mortar as both a construction material and a biological growth medium for algae. This approach combines biochar's physical benefits with the biological process of algae growth, offering a dual-purpose solution for carbon sequestration and sustainable construction practices. By incorporating corn stalk biochar (CSB), a renewable agricultural byproduct, into mortar formulations, this study examines how varying concentrations of biochar influence the mortar's physicochemical properties, such as compressive strength, porosity, and water absorption. In addition to evaluating the mortar's structural performance, the research explores its ability to support the cultivation of *Chlorella* and *Scenedesmus* species. Furthermore, the study assesses the $CO_2$ absorption potential of biochar-enhanced mortars, both with and without algal cultivation, to better understand the added value of integrating biological processes with construction materials. This dual-purpose application not only innovates within the construction sector but also contributes to global sustainability efforts through enhanced carbon capture and renewable energy production, paving the way for scalable, eco-friendly solutions.

## 2. Materials and Methods

### *2.1. Preparation and Characterization of Corn Stalk Biochar*

Corn stalk samples were cut into pieces measuring 5–8 cm in size, thoroughly washed with water, and dried at a temperature of 105 ± 5 °C for 1 h. After drying, the samples were stored in a moisture-free environment to prevent contamination. The biochar synthesis was conducted through pyrolysis at 600 °C for 60 min using a specially assembled pyrolysis furnace with a controlled heating rate of 3 °C $min^{-1}$. The resulting CSB was ground using a crushing machine (GM/EP-100x60X, Guang Ming, Jiangxi, China) followed by a hammer mill (GM/PC400x200A, Guang Ming, Jiangxi, China) to achieve a fine powder that passed through a No. 325 sieve. The CSB sample was then analyzed to assess its various physical and chemical properties.

For particle size distribution, a laser particle size analyzer (CILAS 1190, CILAS, Orléans, France) was used. Surface morphology of the CSB was examined via scanning electron microscopy (SEM) (JEM2100, Merlin Compact, Carl Zeiss, White Plains, NY, USA) at an accelerating voltage of 5.0 kV, providing detailed structural insights. Functional groups present in the CSB were identified through Fourier-transform infrared (FTIR) spectroscopy (Tensor27, Bruker, Karlsruhe, Germany). The elemental composition of the CSB was analyzed using XRF (Malvern Panalytical Ltd., Malvern, UK) and an organic elemental analyzer (Flash 2000, Thermo Scientific, Waltham, MA, USA). Furthermore, the porosity and surface characteristics of the CSB were determined by nitrogen adsorption–desorption isotherms at 77 K, using a micromeritics instrument (ASAP2460, Micromeritics Instrument Co., Ltd., Norcross, GA, USA). As described by Gotore et al. [29], the Brunauer–Emmett–Teller (BET) method was used to calculate the surface area and pore characteristics of the CSB.

### *2.2. Mortar Preparation*

In this study, ordinary Portland cement (OPC) and coarse aggregate were utilized as the primary components for producing Portland cement (PC) mortar. The chemical composition of OPC was determined through X-ray fluorescence (XRF) analysis (Malvern Panalytical Ltd., Malvern, UK) and is summarized in Table 1. The OPC used had a specific gravity of 3.13. River sand, purchased from a local supplier in Songkhla, Thailand, was

selected as the fine aggregate, in accordance with the particle size distribution requirements specified by ASTM C33 [30]. Tap water, with a pH range of 6–7, was used for both mixing and curing the mortar specimens to replicate the conditions typically used in real-world cement and mortar production, rather than deionized water commonly used in laboratory settings.

**Table 1.** Elemental composition of ordinary Portland cement (OPC).

| Element/Compound | Composition (%) ($n$ = 3) |
|---|---|
| Calcium oxide (CaO) | 63.11 ± 1.20 |
| Silicon dioxide ($SiO_2$) | 16.69 ± 0.66 |
| Aluminum oxide ($Al_2O_3$) | 4.40 ± 0.21 |
| Sulfur trioxide ($SO_3$) | 3.51 ± 0.05 |
| Ferric oxide ($Fe_2O_3$) | 3.13 ± 0.04 |
| Organic matter (CHNO) | 5.98 ± 0.08 |
| Magnesium oxide (MgO) | 1.60 ± 0.02 |
| Potassium oxide ($K_2O$) | 0.842 ± 0.001 |
| Sodium oxide ($Na_2O$) | 0.121 ± 0.003 |
| Phosphorus pentoxide ($P_2O_5$) | 0.120 ± 0.004 |
| Titanium dioxide ($TiO_2$) | 0.292 ± 0.005 |
| Strontium oxide (SrO) | 0.074 ± 0.011 |
| Chloride ($Cl^-$) | 0.032 ± 0.006 |
| Copper oxide (CuO) | 0.030 ± 0.004 |
| Zinc oxide (ZnO) | 0.030 ± 0.005 |
| Manganese oxide (MnO) | 0.024 ± 0.007 |
| Arsenic trioxide ($As_2O_3$) | 0.011 ± 0.000 |
| Zirconium dioxide ($ZrO_2$) | 0.013 ± 0.005 |
| Molybdenum trioxide ($MoO_3$) | 0.014 ± 0.004 |
| Rubidium oxide ($Rb_2O$) | 0.004 ± 0.000 |

Control mortar mixtures (CM) were prepared using a blend of OPC, sand, and water. CSB was then added to the mixtures at various weight percentages of OPC, specifically at 2.5%, 5%, 10%, 30%, 50%, and 75%, which were designated as CSB2.5, CSB5, CSB10, CSB30, CSB50, and CSB75, respectively. The water-to-cement and cement-to-sand ratios adhered to the standards outlined by ASTM C109/C109M (water–cement–sand = 0.7:1:2.75) [31], which are used to evaluate the compressive strength of hydraulic cement mortars. In the biochar treatments, 'cement' refers to the total mass of cementitious material, including both OPC and biochar. The water-to-cement and cement-to-sand ratios were maintained according to ASTM C109/C109M, with the cement mass in the biochar mixtures representing the combined mass of OPC and biochar to ensure consistent ratios across all samples. A detailed summary of the mix proportions can be found in Table 2.

**Table 2.** Mix proportions of mortar with and without corn stalk biochar (CSB) used in this study.

| Treatment | OPC (g) | Water (ml) | Sand (g) | CSB (g) |
|---|---|---|---|---|
| CM | 250.0 | 175.0 | 687.5 | - |
| CSB2.5 | 243.8 | 175.0 | 687.5 | 6.3 |
| CSB5 | 237.5 | 175.0 | 687.5 | 12.5 |
| CSB10 | 225.0 | 175.0 | 687.5 | 25.0 |
| CSB25 | 187.5 | 175.0 | 687.5 | 62.5 |
| CSB50 | 125.0 | 175.0 | 687.5 | 125.0 |
| CSB75 | 62.5 | 175.0 | 687.5 | 187.5 |

The ingredients were carefully measured and mixed using a mortar mixer (ELE International, Milton Keynes, UK), following the ASTM C305 standard [32], to ensure a

consistent and uniform mixture. The freshly prepared mortar was then poured into steel molds with dimensions of 5 cm × 5 cm × 5 cm and left to set overnight. After demolding, the specimens were sealed in plastic wrap to preserve moisture and allowed to cure for a period of 28 days. Upon completion of curing, each mix proportion produced 20 specimens that were subjected to a comprehensive series of tests.

### *2.3. Mortar Tests*

Compressive strength testing was performed in full compliance with ASTM C109/C109M [31]. Additionally, six specimens were designated for density measurements using the ASTM C188-17 [33]. Water absorption tests were carried out according to ASTM C1403-15 [34], with water absorption calculated by determining the percentage weight increase of the specimens after immersion in water compared with their dry weight.

The cracked samples, each approximately 1 cm in size, were carefully coated with a thin layer of gold and analyzed using SEM (JEM2100, Merlin Compact, Carl Zeiss, USA) at an accelerating voltage of 5.0 kV to reveal their structural characteristics. In addition, FTIR spectroscopy (Tensor27, Bruker, Karlsruhe, Germany) was performed over a wavenumber range of 500–4000 $cm^{-1}$, with 64 scans and a spectral resolution of 4 $cm^{-1}$. Samples were prepared by mixing 10 wt% in KBr and pressed into pellets. All the tests were performed in three replicates.

### *2.4. Microalgae Cultivation on CSB-Enhanced Mortar Specimens*

#### 2.4.1. Initial Cultivation of Algae for Biomass Expansion Before Mortar Transfer

This study aimed to expand the quantity of algae, specifically the *Chlorella* and *Scenedesmus* species, both of which are highly effective in capturing $CO_2$ emissions, and to monitor changes during their cultivation. These species were chosen due to their fast growth rates, high $CO_2$ fixation capacity, and resilience under varying environmental conditions [35,36]. Additionally, both *Chlorella* and *Scenedesmus* have the ability to produce high biomass, making them suitable candidates for biofuel production and other industrial applications.

*Chlorella* sp. (TISTR 8262) and *Scenedesmus* sp. (TISTR 9384) were obtained from the Algal Excellence Center (ALEC) in Thailand. A batch experiment was conducted by inoculating *Chlorella* sp. and *Scenedesmus* sp. into BG11 liquid medium. The initial algal cell density was determined using a spectrophotometer (Cary 60, Agilent, Waldbronn, Germany) at a wavelength of 560 nm, with the optical density ($OD_{560}$) recorded at approximately 0.8. Subsequently, 14 mL of the inoculated sample was transferred into a 2 L photobioreactor containing 1 L of liquid medium to enhance biomass production. The culture was continuously illuminated with warm white light (LX-73, Digicon Technology Co., Ltd., Taichung, Taiwan) at an intensity of approximately 4000 lux and maintained at a temperature of 25 °C for 24 h. Continuous aeration was provided at a rate of 30 L $min^{-1}$ using an air pump (AP-10, Shenzhen Yamano Aquariums Co., Ltd., Guangdong, China) to maintain suspension and prevent sedimentation in the culture (Figure 1a).

The algae were cultured until their $OD_{560}$ reached 4.0, after which they were transferred to mortar surfaces for further growth. A 16-day inoculation period was used to monitor algal growth (Figure 1b), with pH levels consistently tracked throughout the experiment. Additionally, aliquots were removed at regular intervals, dried, and weighed to assess biomass accumulation.

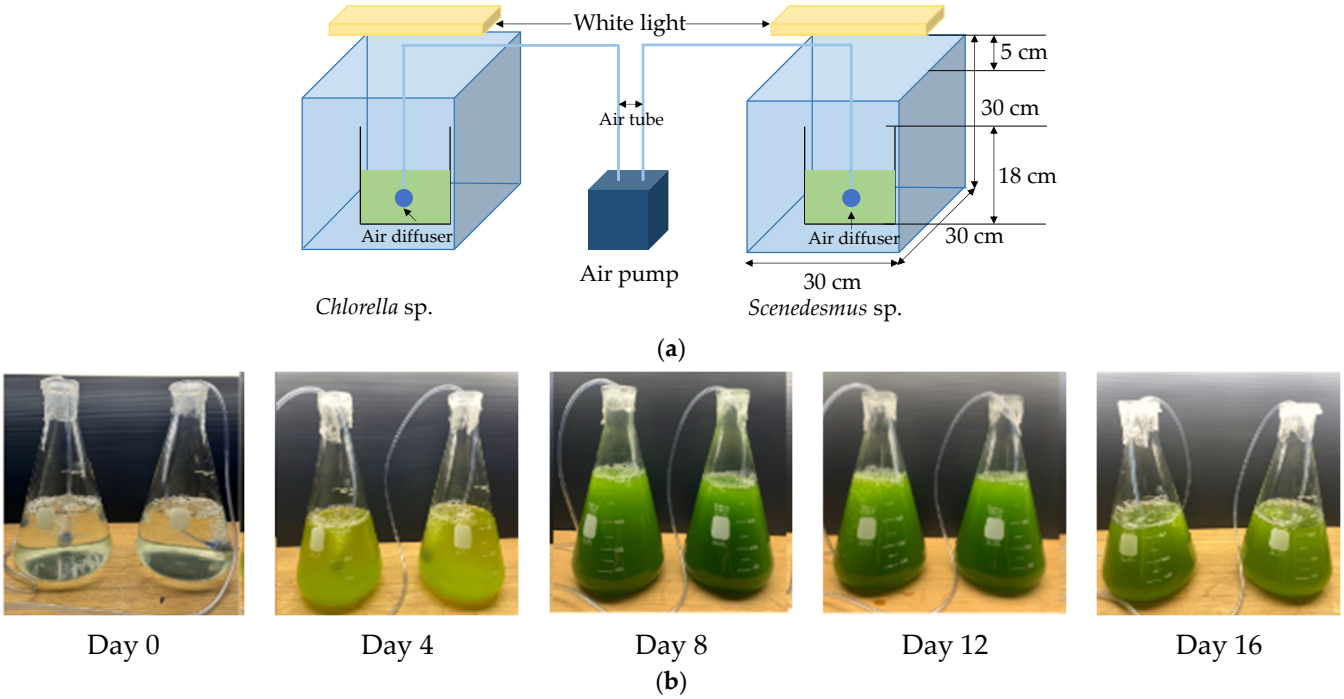



**Figure 1.** Cultivation system for *Chlorella* sp. (TISTR 8262) and *Scenedesmus* sp. (TISTR 9384) (**a**), and the algae growth progression from day 0 to day 16 (**b**).

#### 2.4.2. Surface Cultivation of Algae on Corn Stalk Biochar-Enhanced Mortar

The process for cultivating both algal species on the surface of mortar blocks involved the following steps: First, the mortar specimens were sanitized using 70% alcohol to reduce potential contaminants and then dried for one hour at a temperature of 60 °C to remove moisture and further inhibit microbial growth, creating a suitable environment for algal cultivation. On the day the algae were ready for cultivation on the CSB-enhanced mortar, 15 mL samples from both algal species were collected and transferred into centrifuge tubes. The samples were centrifuged at 2012× *g* for 5 min. After centrifugation, 1 g of the algal biomass was extracted and suspended in 1 mL of fresh BG11 culture medium. All mortar specimens were soaked in fresh BG11 medium to maintain sufficient moisture levels. The resuspended algal cells were uniformly applied to the top surfaces of the mortar specimens. The mortar specimens were then placed on Petri dishes, and the medium level was maintained at a constant depth of 2 cm by replenishing it daily throughout the cultivation period. This consistent medium level was necessary to ensure the algae had a stable moisture environment, which is crucial for their growth and metabolic activity. Maintaining adequate moisture prevents desiccation and helps facilitate nutrient exchange between the algae and the medium. Subsequently, the specimens were placed in a sanitized, sealed chamber, maintained at 25 °C, and exposed to a consistent light source with an intensity of 4000 lux. A glass container measuring 30 × 30 × 30 $cm^3$ was used for this setup. The arrangement of the light source and mortar samples is shown in Figure 2a.

#### 2.4.3. Assessment of Algal Growth and Their Carbon Dioxide Absorption Capacity

The quantity of algal growth was indirectly determined by measuring changes in dried biomass during the cultivation period. Biomass was measured by drying the entire mortar samples in an oven at 105 °C for 24 h, and the recorded weights were used to quantify algae growth on the mortar surface. The experiment was conducted in triplicate to ensure the reliability of the results. Visual observations were captured using a Canon EOS 80D digital camera (Tokyo, Japan) equipped with an EF-S 18-135 IS USM lens. The camera settings

included ISO 800, a shutter speed of 1/2000, and an aperture of F8.0. The distance between the lens and the surface of the sample was 10 cm. The photos were taken in a dark room with external lighting.

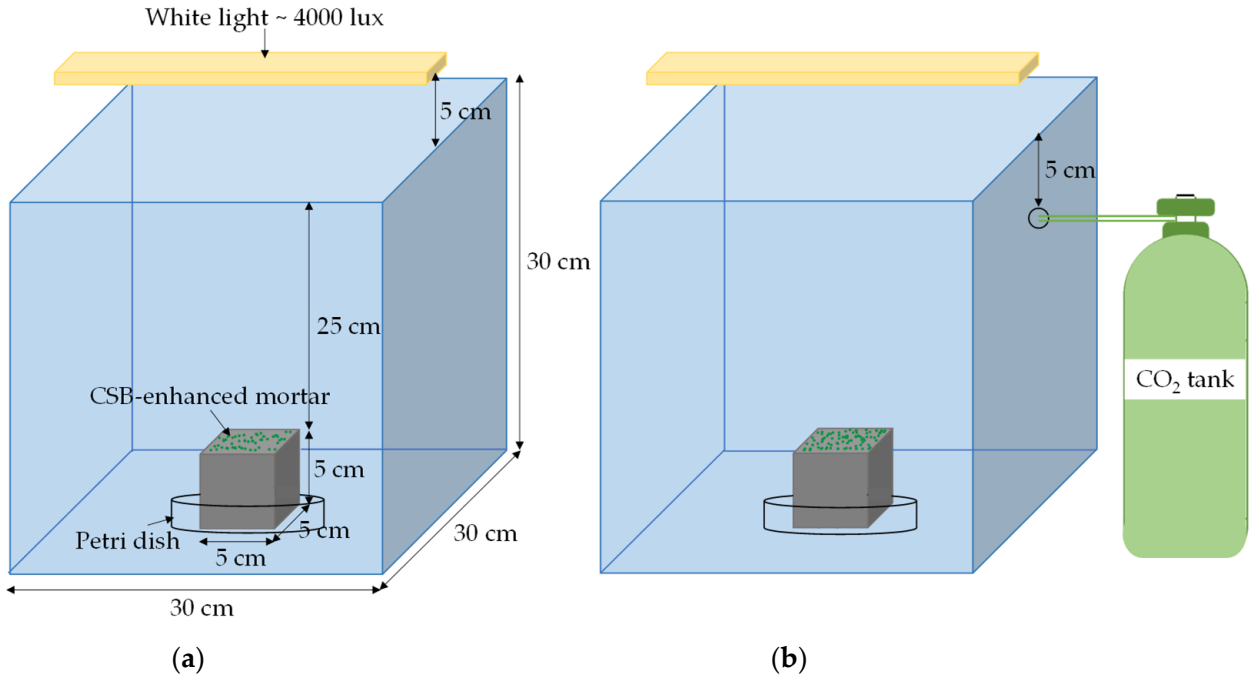



**Figure 2.** Illustration of the setup for cultivating both algal species on the surface of mortar blocks within a sanitized chamber (**a**) and the $CO_2$ sequestration test (**b**).

To assess $CO_2$ absorption efficiency, algae were cultivated on mortar specimens enhanced with different concentrations of CSB, while CSB-enhanced mortars without algae were used as the control for comparison. On the day of maximum growth, as indicated by dried biomass weight, was recorded, the mortar specimens were transferred to a sanitized, sealed chamber maintained at 25 °C with continuous illumination at an intensity of 4000 lux. To maintain moisture levels, each mortar specimen was placed on a Petri dish, ensuring the medium depth remained constant at 2 cm. No additional medium was added during the experiment. Afterward, pure $CO_2$ (99%) was introduced into the chamber at a controlled flow rate of 0.05 $m^3$ $m^{-3}$ $min^{-1}$ for 2 min using a gas infusion pump (Watson Marlow Model 502S, WMFTG, Cornwall, UK). $CO_2$ concentrations were measured at both the inlet (influent $CO_2$) and outlet (effluent $CO_2$) using a gas analyzer (Biogas 5000, Geoteck, West Midlands, UK). These measurements were taken every 2 days over a 16-day period to monitor $CO_2$ alterations. The experiment was performed in triplicate to ensure accuracy and reproducibility.

To calculate the $CO_2$ absorption ratio, $W_0$ (g) represents the total mass of $CO_2$ supplied or injected into the chamber for absorption by the algae/mortar system. The amount of $CO_2$ absorbed by the system ($W_1$, g) was then calculated using the following equation, adapted from the study by Yin et al. [37]:

$$W_1 = \frac{44(C_0 - C_1)}{V} \quad (1)$$

where $C_0$ and $C_1$ represent the initial and final concentrations of $CO_2$ in the system (mmol $m^{-3}$), respectively, and V denotes the volume of the container ($m^3$).

The $CO_2$ absorption ratio (R) was calculated using the following formula:

$$R = \frac{W_1}{W_0} \times 100\% \quad (2)$$

It should be noted that this ratio is expressed as a percentage, with values close to 0 indicating minimal $CO_2$ absorption and values approaching 100 indicating substantial $CO_2$ absorption.

### *2.5. Data Analysis*

The impact of varying levels of CSB on the physical and mechanical properties of the mortar as well as on the growth of algae was assessed using the General Linear Model (GLM) in SAS software (version 9.4, SAS, 2002). Fisher's least significant difference (LSD) test was employed to compare the treatment means, with significance set at the 5% probability level.

## 3. Results and Discussion

### *3.1. Characterization of Corn-Stalk Biochar*

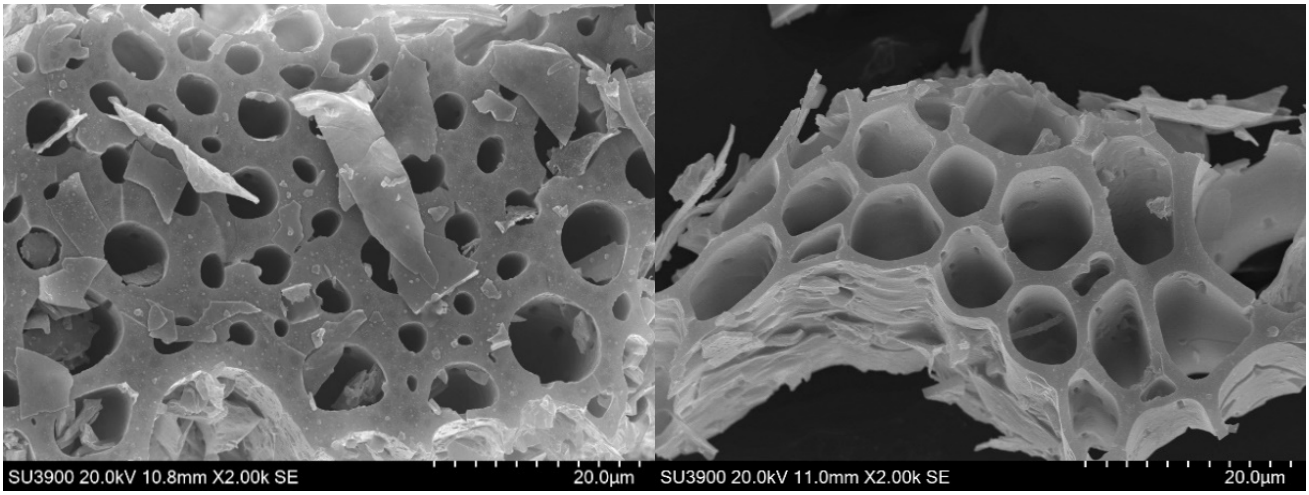
Table 3 summarizes the elemental composition and characteristics of CSB, which contains 62.3% carbon, typical of biochar produced via pyrolysis [38]. The low hydrogen content (3.5%) indicates stability and resistance to decomposition, while the moderate oxygen content (22.3%) suggests the presence of reactive oxygen-containing groups. The relatively high nitrogen content (9.3%) makes CSB suitable for agricultural applications and the adsorption of nitrogenous pollutants. Although the sulfur content is low (3.1%), it still contributes to the material's overall reactivity. The elemental ratios, including a low O/C ratio and H/C ratio, highlight the high degree of carbonization and structural stability of CSB. Wang et al. [39] noted that the elemental composition of corn biomass can vary naturally at different levels, including between and within species, as well as among different plant components. These variations are influenced by factors such as growth conditions and environmental stress. Furthermore, the large surface area (680.3 $m^2\ g^{-1}$) and mesoporous structure (average pore diameter of 1.9 nm) suggest a strong potential for efficient pollutant adsorption and gas capture. The $CO_2$ absorption capacity (2.9 mmol $g^{-1}$) further emphasizes the material's potential to reduce atmospheric $CO_2$ and support carbon sequestration initiatives.

**Table 3.** Elemental composition and physical properties of corn stalk biochar (CSB).

| Parameter | Value ($n$ = 3) |
|---|---|
| Carbon (C, %) | 62.3 ± 0.1 |
| Hydrogen (H, %) | 3.5 ± 0.0 |
| Oxygen (O, %) | 22.3 ± 0.2 |
| Nitrogen (N, %) | 9.3 ± 0.1 |
| Sulfur (S, %) | 3.1 ± 0.0 |
| O/C ratio (-) | 0.4 ± 0.0 |
| H/C ratio (-) | 0.006 ± 0.006 |
| C/H ratio (-) | 18.1 ± 0.1 |
| Surface area ($m^2\ g^{-1}$) | 680.3 ± 2.6 |
| Total pore volume ($cm^3\ g^{-1}$) | 0.4 ± 0.3 |
| Average pore diameter (nm) | 1.9 ± 0.1 |
| $CO_2$ absorption capacity (mmol $g^{-1}$) | 2.9 ± 0.0 |

SEM images reveal the morphological characteristics of CSB (Figure 3a,b), showing a mix of large and small pores with diameters ranging from 2 to 10 µm. The pore distribution

appeared irregular and uneven, highlighting the natural structural characteristics of the CSB. It is worth noting that the biochar was not subjected to acid- or base-cleaning treatments to remove impurities, a step that could have further refined the pore structure. However, this decision was made as a cost-saving measure, simplifying the production process while still preserving sufficient porosity for practical applications. Despite the absence of additional treatments, the CSB maintains a functional pore structure suitable for various environmental uses, such as pollutant adsorption and gas capture [40].




(**a**) (**b**)

**Figure 3.** Surface morphology and porosity of corn stalk biochar (CSB) at 2000× (**a**) and 5000× (**b**) magnifications, respectively.

The BET analysis of the CSB sample, presented in Figure 4a, provides valuable insights into its surface area and adsorption characteristics. The adsorption curve exhibits a rapid increase in gas volume at lower relative pressures ($P/P_0$), eventually reaching a plateau near 1.0, indicating that the CSB has a high adsorption capacity, particularly at lower pressures. At near-saturation pressures, the maximum adsorption volume is approximately 250 $cm^3\ g^{-1}$ STP. This behavior highlights the biochar's substantial surface area and pore structure, which are crucial for adsorbing gases such as $CO_2$, making it suitable for carbon sequestration applications [41]. In contrast, the desorption curve shows a gradual decrease in adsorbed gas volume as the relative pressure declines. The observed hysteresis between the adsorption and desorption curves suggests the presence of micropores and mesopores within the biochar. This hysteresis phenomenon is typical of materials that can trap adsorbed gases even when the pressure decreases, thereby enhancing the material's ability to store and sequester gases such as $CO_2$ [42]. The unique pore structure of CSB makes it a promising material for $CO_2$ sequestration and other gas storage applications.

The functional groups present on the surface of the CSB as identified through FTIR analysis are illustrated in Figure 4b. A variety of key functional groups were identified, each contributing to the biochar's overall chemical properties. The O–H bond, which is indicative of hydroxyl groups, was observed at 3437 $cm^{-1}$, suggesting the presence of alcohol or phenol groups that could enhance the biochar's reactivity and adsorption potential [43]. Additionally, the C–H bond corresponding to alkyl hydrocarbons was detected at 2921 $cm^{-1}$, which is typical of long carbon chains and organic compounds [44,45]. A distinct carbonyl group (C=O bond) was identified at 1627 $cm^{-1}$, indicating the presence of ketones, aldehydes, or carboxylic acids [46]. The shoulder observed at 1550 $cm^{-1}$ may indicate the presence of carboxylate groups, which could contribute to the biochar's ability to bind with metals or enhance its adsorption properties, depending on the pyrolysis conditions [47]. The

analysis also revealed an aromatic C=C bond at 1384 $cm^{-1}$, highlighting the presence of stable aromatic structures that form during pyrolysis [48]. This stability is critical for the biochar's long-term durability in environmental applications. The C–O stretching vibration was detected at 1262 $cm^{-1}$, contributing to the variety of functional groups involved in the adsorption and chemical reactivity of the carbon materials [49]. Likewise, the presence of a Si–O bond at 1104 $cm^{-1}$ suggests the incorporation of silicon oxide and potentially $SO_2$ compounds, which might be remnants of inorganic material from the corn stalks. Wang et al. [39] indicated that the silicon content in CSB, predominantly found in cereals and crop species, forms a silicate network structure and a silicate skeleton on the external surface of the stalk or stem. This is supported by the appearance of a shoulder at 1050 $cm^{-1}$, further indicating potential silicon-containing compounds or oxygenated functional groups that contribute to the material's adsorption potential [49]. Finally, the C–H bending vibration for aromatic structure appeared at 873 $cm^{-1}$ and 794 $cm^{-1}$ [38,50]. These diverse functional groups on the surface of CSB play a crucial role in its adsorption capabilities and environmental reactivity.

### *3.2. Physicochemical Properties of CSB-Enhanced Cement Mortar*

#### 3.2.1. Compressive Strength

The compressive strength of cement mortar was notably affected by varying concentrations of CSB, as shown in Figure 5a, with distinct percentage changes observed relative to the CM sample. At a lower concentration of 2.5%, a modest 3.5% increase in compressive strength was recorded. This finding is consistent with the results of studies conducted by Gupta and Kua [51] and Wang et al. [52], which demonstrated that the incorporation of 1% w $w^{-1}$ biochar into cement mortar enhanced the formation of cement hydrates, leading to compressive strength increases of 16% and 9%, respectively, compared with plain mortar. Similarly, Zhao et al. [53] observed that low biochar dosages (less than 2.5% of binder weight) improved compressive strength by 6% and 7% at 7 and 28 days, respectively. Research by Liu et al. [54] on cement composites containing bamboo biochar also reported an increase in compressive strength and crack resistance, with an optimal biochar content of 1–3% due to the material's filling and self-curing effects. These improvements in mechanical strength can be attributed to the formation of additional cement hydrates, primarily calcium silicate hydrate (C–S–H) and calcium aluminate hydrate (C–A–H) gels, which strengthen the overall mortar matrix [55,56].

As the concentration of biochar increases, a significant decrease in compressive strength is observed ($p < 0.05$). When CSB content reaches 5% or higher, biochar begins to interfere with the cementitious matrix, functioning more as a porous, inert filler rather than contributing to structural reinforcement. This leads to a significant 31.3% reduction in strength at 5% CSB, which further escalates to a 57.3% reduction at 10%. With a CSB concentration of 25%, the strength diminishes by 81.9%, as biochar starts to replace a substantial portion of cement, thereby disrupting hydration and matrix formation. At even higher concentrations, such as 50% and 75%, biochar dominates the mixture, resulting in a compressive strength loss of over 95%, critically weakening the mortar's structural integrity. These findings are consistent with studies by Praneeth et al. [14] and Akhtar and Sarmah [57], who observed that when biochar is added beyond a certain limit, the volume of hydration products filling the pores becomes insufficient relative to the larger pore sizes of the biochar. This leads to increased porosity instead of a denser matrix, which ultimately results in a reduction in compressive strength across all mixtures.

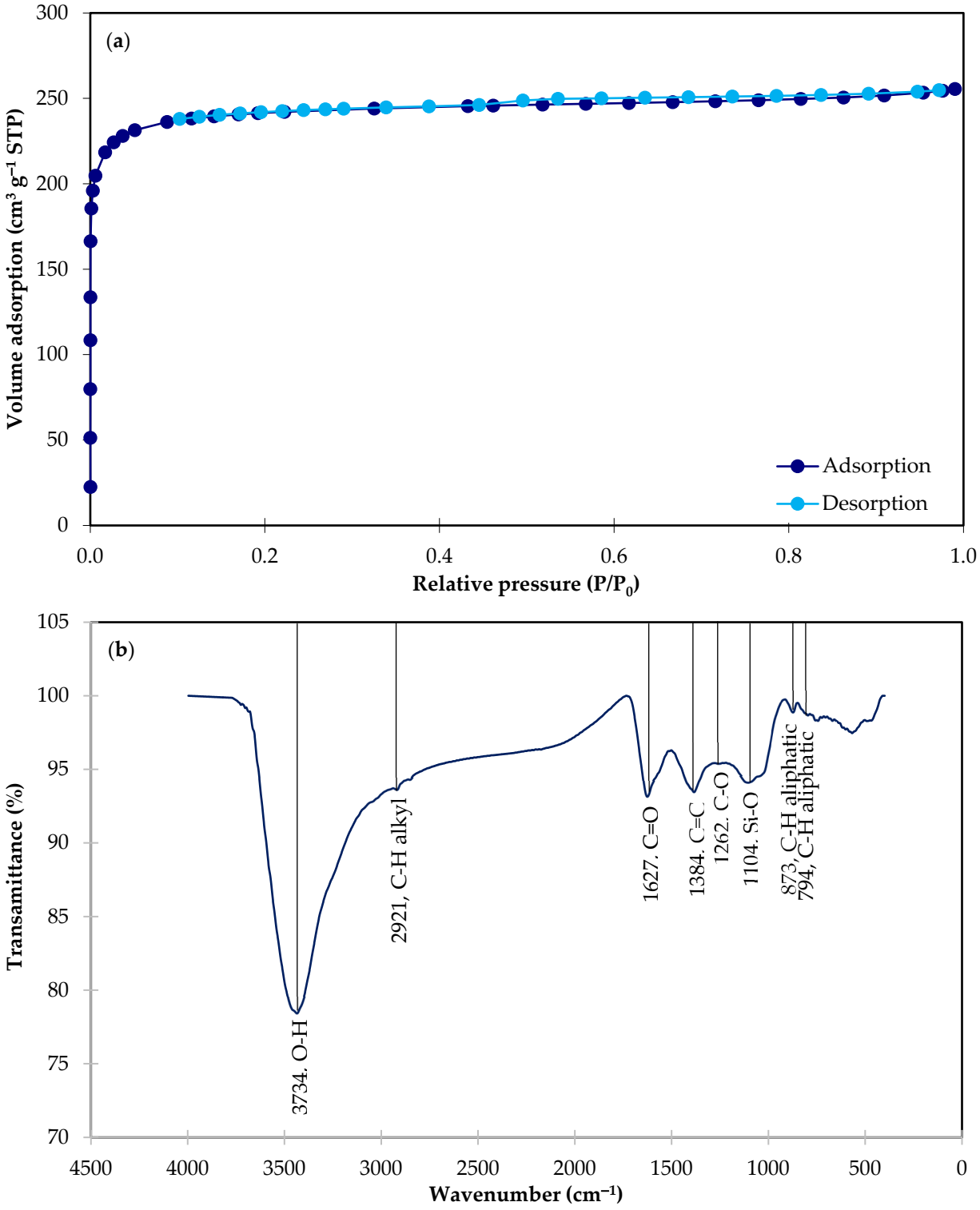



**Figure 4.** BET analysis (**a**) showing the surface area and pore size distribution of corn stalk biochar (CSB) and FTIR spectrum (**b**) illustrating the functional groups present on the surface of CSB.

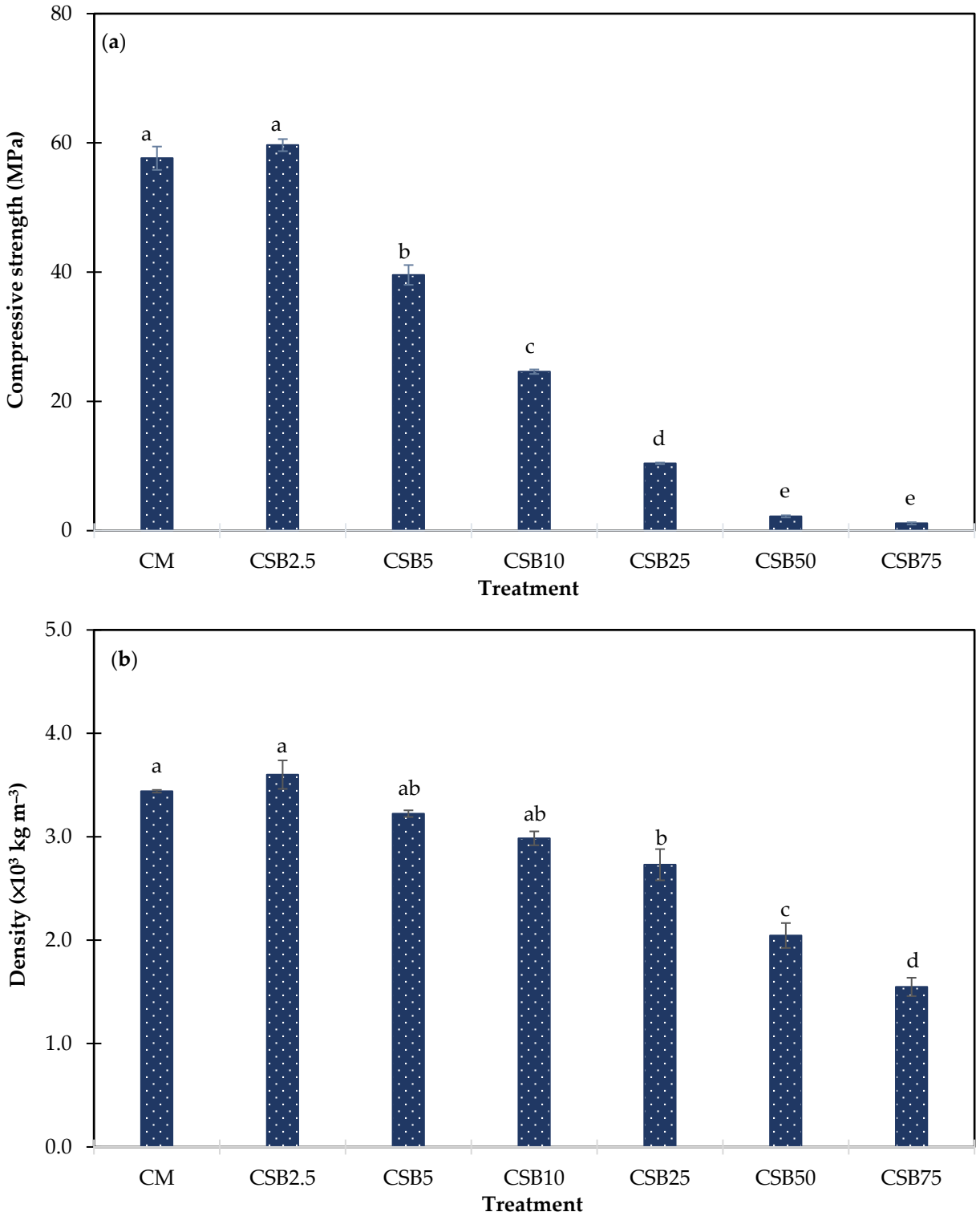



**Figure 5.** *Cont.*

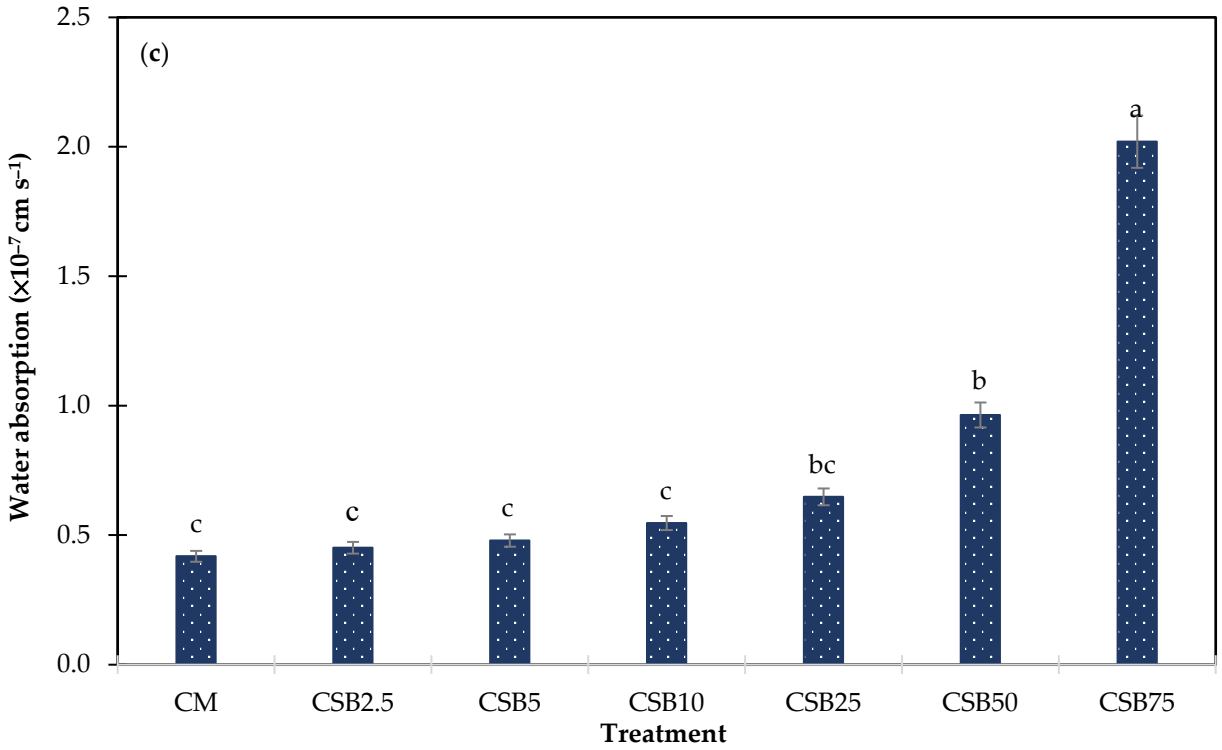



**Figure 5.** Impact of corn stalk biochar (CSB) at various levels on the compressive strength (**a**), density (**b**), and water absorption (**c**) of cement mortar. Means (±standard deviation) within a bar graph marked with distinct letters signify significant differences according to the LSD test ($p < 0.05$).

#### 3.2.2. Density

The incorporation of CSB into cement mortar significantly affects this property (Figure 5b). At a low concentration of 2.5% CSB, the density increases by 4.7% compared with the CM sample. However, as the CSB content increases, a decline in density is observed. For instance, at 5% CSB, the density decreases by 6.4%, and this reduction becomes more pronounced at 10% CSB, where a 13.4% drop is recorded. The decrease continues to intensify at 25% CSB, with a significant 20.6% reduction ($p < 0.05$). At very high concentrations, such as 50% and 75% CSB, the density sharply declines, with reductions exceeding 40%.

The initial increase in density observed at 2.5% CSB can be explained by the biochar's ability to fill small voids within the cement matrix. This enhances particle packing, resulting in a denser structure. However, as the biochar content rises beyond 5%, the material becomes lighter and more porous due to the lack of sufficient binding and cohesion between biochar particles and the cement matrix. This leads to a marked reduction in density. Brewer et al. [58] noted that the reduction in bulk density is closely tied to an increase in void spaces within the composite. Since biochar has a lower density than cement and sand, its incorporation reduces the overall bulk density of the mixture. Furthermore, the porous nature of biochar itself contributes to the introduction of additional voids around its particles when integrated into the cement matrix, further diminishing the bulk density [14,59].

#### 3.2.3. Water Absorption

The incorporation of CSB into cement mortar results in a progressive increase in water absorption, with the rise becoming more pronounced as the biochar content increases (Figure 5c). At a low concentration of 2.5% CSB, water absorption increases by 8.0% compared with the control. As the biochar content reaches 5%, water absorption rises to 14.5%, and when the concentration is further increased to 10%, it jumps to 30.7%, as

biochar begins to dominate the mortar matrix and creates more voids. With a 25% CSB concentration, water absorption increases significantly, reaching 55.0%. This trend becomes even more pronounced at 50% CSB, where water absorption escalates by 130.4%. At the highest concentration of 75% CSB, water absorption soars to 382.8%, as the biochar fully dominates the mixture, resulting in a highly porous and water-retentive mortar.

A plausible explanation for these results is that the porous structure of biochar particles did not facilitate the creation of a denser surface but rather increased the capillary pores, leading to higher water absorption [57,60]. This observation aligns with Akinyemi and Adesina [61], who found a strong linear relationship between water absorption and the porosity of mortar mixtures incorporating biochar. Additionally, biochar's high water retention capacity enables it to absorb and retain significant amounts of water, further contributing to the elevated water absorption levels in the composites. The particle size of biochar also plays an important role—larger particles may be less effective at filling voids, reducing the potential for densification and resulting in a greater number of pores, which ultimately increases water absorption [14].

### *3.3. Algal Growth Dynamics*

#### 3.3.1. Increment of Optical Density

The OD measurements for both *Chlorella* sp. and *Scenedesmus* sp. exhibited distinct growth patterns over the 16-day cultivation period (Figure 6a). *Chlorella* sp. began with an OD of 0.80 on day 0 and steadily increased, peaking at 4.1 on day 8—an overall increase of 415%. However, by day 10, the OD had dropped by 6% from its peak, and by day 16, it had declined by 32%. Similarly, *Scenedesmus* sp. started at an OD of 0.80 on day 0, reaching its maximum of 4.2 on day 8, representing a 423% increase. By day 10, its OD had decreased by 2%, and by day 16, it had declined by 17%. These increases during the first 8 days indicate the exponential growth phase for both species, after which they transitioned into the stationary or decline phases. The growth phase plays a critical role in influencing the photosynthetic activity of both algae species, as highlighted by Oukarroum [62]. As cultures approach the stationary phase, photosynthetic rates tend to decrease, likely due to nutrient depletion and the accumulation of metabolic byproducts within the culture medium. Additionally, as algal biomass increases, light availability can become a limiting factor, further affecting photosynthetic efficiency. Reduced light penetration can diminish electron flow in the photosynthesis process, as noted by Falkowski and Raven [63], which contributes to the overall decline in photosynthetic activity as the cultures age. These combined factors—nutrient limitations, byproduct accumulation, and restricted light availability—create a challenging environment for sustained photosynthesis in older cultures.

The more rapid decline in *Chlorella* sp. compared with *Scenedesmus* sp. could be attributed to species-specific metabolic differences, which may cause *Chlorella* sp. to enter the stationary- or decline-phase sooner. In contrast, *Scenedesmus* sp. tends to sustain its biomass for a longer period, possibly due to its more efficient nutrient utilization or greater tolerance to environmental stress as the culture ages. This aligns with the findings of Zhang et al. [64], who observed that *Scenedesmus* exhibited stronger resistance to stress than *Chlorella* in a co-culture system. They noted that *Scenedesmus* cells typically form wedge-shaped, four-cell consortia, whereas *Chlorella* cells remain dispersed and separate in suspension. The aggregation of *Scenedesmus* may offer an adaptive advantage, enabling it to withstand environmental stressors more effectively. Shaima et al. [65] similarly noted that microalgae growth rates are linked to their adaptability, with higher growth rates reflecting a species' ability to thrive under specific environmental conditions. These observations

are consistent with Sabatini et al. [66], who also highlighted the superior resilience of *Scenedesmus* under stress conditions.

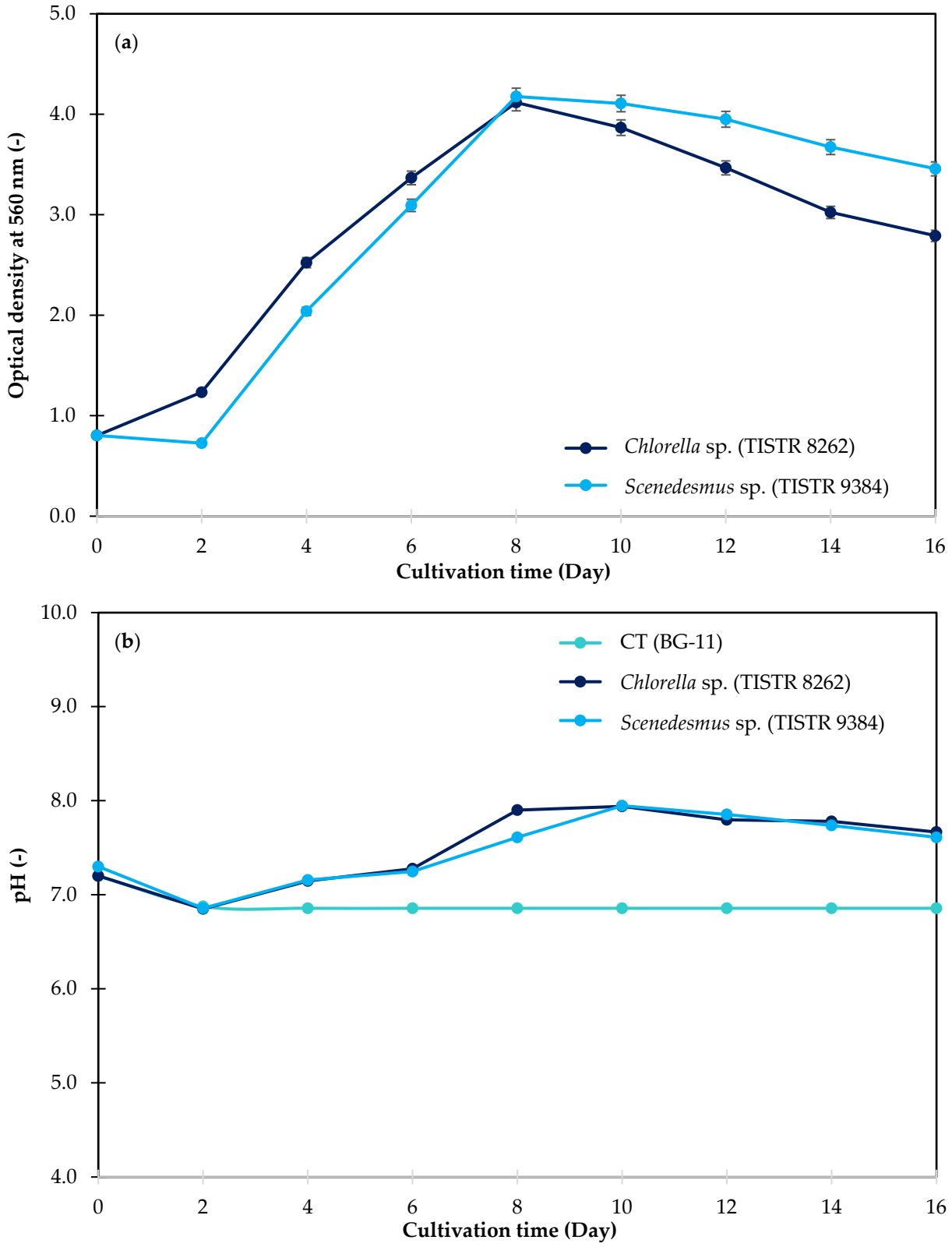



**Figure 6.** *Cont.*

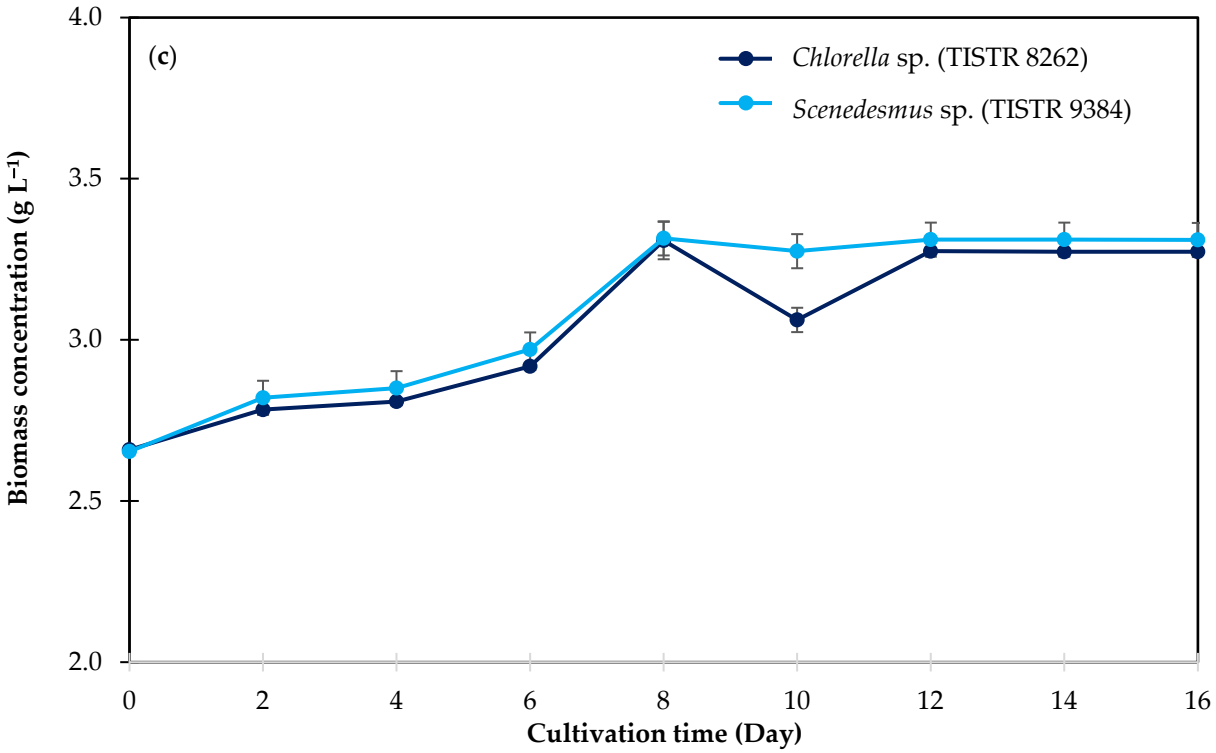



**Figure 6.** Variations in optical density (**a**), pH (**b**), and biomass (**c**) during the cultivation of *Chlorella* sp. (TISTR 8262) and *Scenedesmus* sp. (TISTR 9384) in the medium.

#### 3.3.2. pH Variations

Throughout the 16-day cultivation period of *Chlorella* sp. and *Scenedesmus* sp. in a liquid medium, noticeable changes in pH were observed, with both species displaying similar trends (Figure 6b). In contrast, the control (CT-BG11) maintained a stable pH throughout the experiment. At the beginning of the cultivation, the pH for both *Chlorella* and *Scenedesmus* was around 7.2–7.3. During the first two days, the pH dropped slightly to just below 6.9. However, after day 2, the pH began to steadily rise for both species, signifying an increase in photosynthetic activity. By day 8, the pH for *Chlorella* had reached 7.9, while *Scenedesmus* reached 7.6, indicating efficient $CO_2$ absorption. By day 10, both species had peaked at similar pH levels (~8.0), marking their period of maximum photosynthetic activity. After day 10, the pH gradually stabilized around 7.6 by day 16, suggesting that both species had reached a steady state of $CO_2$ uptake and metabolic equilibrium. In contrast, the control (CT-BG11) exhibited no significant pH fluctuations, remaining around 6.9 for the entire 16-day period. This stability in the control confirms that the pH changes in the algae cultures were primarily driven by their metabolic activities, specifically $CO_2$ uptake during photosynthesis.

The initial drop in pH is likely due to early metabolic activity, during which the algae absorb $CO_2$ and release organic acids as metabolic byproducts, increasing the acidity of the medium. This pH decrease is typical in the early stages of algal growth as the cells adjust to their environment and begin utilizing nutrients [67]. As photosynthesis progresses, the pH begins to rise due to the reduction in dissolved $CO_2$ and carbonic acid [68,69], indicating efficient $CO_2$ absorption by the algae. This upward trend in pH highlights the effectiveness of both algae species in capturing $CO_2$ through photosynthesis.

#### 3.3.3. Biomass Accumulation

The comparison of biomass accumulation between *Chlorella* sp. and *Scenedesmus* sp. over the 16-day cultivation period reveals distinct differences in their growth dynamics

(Figure 6c). At the start of the experiment (day 0), the biomass of both species was nearly identical, with *Chlorella* sp. at 2.66 g $L^{-1}$ and *Scenedesmus* sp. at 2.65 g $L^{-1}$. By day 4, *Scenedesmus* sp. exhibited a 12% increase in biomass, slightly exceeding the 10% increase shown by *Chlorella* sp. This gap widened by day 8, when *Scenedesmus* sp. achieved a 25% increase in biomass, compared with the 15% growth observed for *Chlorella* sp. Throughout the cultivation period, *Scenedesmus* sp. maintained its lead in biomass production, and by day 16, its overall growth reached 25%, while *Chlorella* sp. exhibited a 23% increase.

The early divergence in growth rates between *Scenedesmus* sp. and *Chlorella* sp. can be attributed to several key physiological differences, particularly in their response to environmental conditions like light and nutrient availability. *Scenedesmus* sp. appears to have a slight advantage in nutrient uptake efficiency and faster adaptation to the culture conditions [62]. During the exponential growth phase around day 8, when cell division and nutrient consumption are at their highest, *Scenedesmus* sp. significantly outperformed *Chlorella* sp., suggesting its superior ability to thrive under these conditions. According to Masojídek et al. [70], *Scenedesmus* sp. exhibits a more effective non-photochemical quenching (NPQ) mechanism, which allows it to handle excess light energy more efficiently. NPQ, regulated by the xanthophyll cycle, helps dissipate excess light energy as heat, protecting the cells from light-induced stress [71]. In contrast, *Chlorella* sp. has a larger antenna system, making it less efficient in quenching excess light, which can lead to reduced photosynthetic capacity under high light conditions [70]. Additionally, *Scenedesmus* sp. has physiological traits, such as the ability to form cell aggregates, as noted by Zhang et al. [64]. This aggregation may offer an advantage in nutrient-rich environments, allowing *Scenedesmus* sp. to sustain higher biomass accumulation over time.

Although OD is commonly used to monitor algal biomass, in this study, the growth trends observed through biomass measurements aligned with the OD data up until day 8 (Figure 6c). Both *Chlorella* and *Scenedesmus* exhibited a peak in OD at this point, corresponding to their exponential growth phase. However, despite the subsequent decrease in OD after day 8, the biomass remained stable. This phenomenon may be attributed to factors such as cell aggregation, pigment degradation, or changes in cell size [72–74]. Oukarroum et al. [62] explained that when *Chlorella* and *Scenedesmus* enter the stationary phase, their maximum photosynthetic performance declines, leading to pigment loss or changes in cell morphology. These alterations reduce light scattering efficiency, causing a decline in OD even though the overall biomass remains stable or continues to increase.

### *3.4. Algal Growth on Cron Stalk Biochar-Enhanced Mortar and Their Efficiency in $CO_2$ Sequestration*

#### 3.4.1. Growth of Chlorella and Scenedesmus Species

In this study, the growth of algae on CSB-enhanced mortars was tracked by measuring changes in dried biomass over a 16-day period, providing insights into the effects of biochar concentrations on algal cultivation (Figure 7a,b). The growth of both algae on cement mortar, even in the absence of CSB, can be attributed to certain material-related physical factors that enhance the bio-receptivity of the surface. These factors include porosity, surface roughness, and the mineral composition of the mortar [75–77]. A rougher surface increases the adherence and retention of microalgae, promoting their growth over time. In addition, the mineral composition of the mortar plays a crucial role in its bio-receptivity. Specific minerals, such as calcite and silica present in the cementitious substrate, can provide essential nutrients that encourage algal colonization [22].

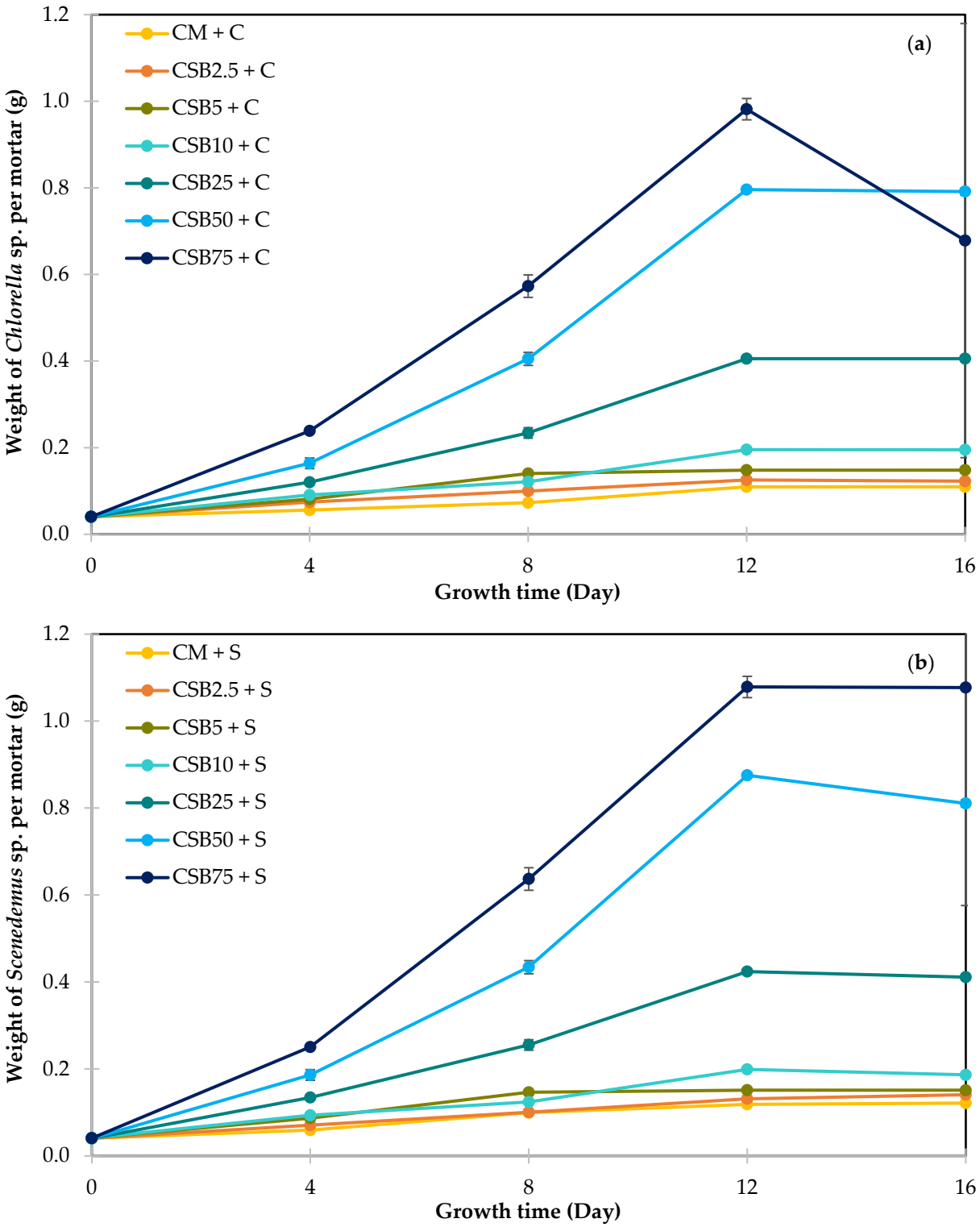



**Figure 7.** Changes in biomass weight of *Chlorella* sp. (TISTR 8262) (**a**) and *Scenedesmus* sp. (TISTR 9384) (**b**) during cultivation on corn stalk biochar (CSB)-enhanced mortar at varying concentrations.

When cultivated on CSB-enhanced mortars, both species of algae exhibited notable growth trends (Figure 7a,b). Under control conditions, *Chlorella* sp. showed a 2.7-fold increase in biomass by day 12, while *Scenedesmus* sp. achieved a slightly higher increase of 2.9-fold, indicating that both species thrived in the absence of biochar. At lower biochar concentrations (CSB2.5 + C/S and CSB5 + C/S), the growth of both species remained moderate, with biomass increases ranging from 3.0- to 3.7-fold for *Chlorella* sp. and 3.5-

to 3.7-fold for *Scenedesmus* sp. by day 16. However, at higher biochar concentrations, algae displayed more pronounced growth, particularly by day 12. *Chlorella* sp. reached a maximum increase of 19.7-fold at CSB50 + C, while *Scenedesmus* sp. achieved an even higher 21.6-fold at CSB50 + S, highlighting the positive effect of biochar in promoting algal growth. At the highest biochar concentration (CSB75 + C/S), both species reached their peak growth, with *Chlorella* sp. showing a 24.2-fold increase and *Scenedesmus* sp. surpassing it with a 26.6-fold rise by day 12. A visual comparison of algal growth on CSB-enhanced mortar between day 0 and day 16 is presented in Figure 8. The observations confirm that mortar with higher biochar content supports increased algal growth over time.

While a very few studies have explored the use of biochar as a medium for algae cultivation, none have investigated its inclusion in mortar formulations. The enhanced growth of algae observed in CSB-enhanced mortars can be attributed to several factors. For instance, Behl et al. [25] demonstrated that adding biochar to the nutrient medium for cultivating *Chlorella pyrenoidosa* in an aqueous solution of Direct Red 31 dye significantly enhanced algal growth. This improvement was attributed to the biochar's richness in essential micronutrients, including manganese (Mn), zinc (Zn), titanium (Ti), iron (Fe), and copper (Cu). However, the specific micronutrient content of biochar can vary depending on the feedstock and pyrolysis conditions. While similar effects may be expected with CSB, further analysis is required to confirm its nutrient composition.

Moreover, when higher doses of biochar are applied, the positive effects on microbial growth become more pronounced. The increased surface area provides additional attachment sites and greater access to nutrients, creating more favorable conditions for microbial proliferation [78,79]. Biochar's porous structure, as described above, also aids water retention [78], further supporting the growth of algae and other microorganisms. Kholssi et al. [80] suggested that the increase in biomass observed in such conditions is not solely due to the rise in algal cell numbers but also to the production of extracellular polymeric substances (EPS), which include polysaccharides, proteins, lipids, and nucleic acids. These EPS enhance the adhesion between biochar and algae, facilitating the formation of an immobilized complex, as similarly noted by Shen et al. [81]. The composition of EPS, which involves hydrophobic interactions, hydrogen bonding, and ionizable groups [79,82,83], likely strengthens the attachment of algae to biochar. Moreover, physical surface attachment is influenced by several factors, including electrostatic forces and the metal ion content present on biochar surfaces [84]. Hill et al. [79] indicated that biochar's surface area and adsorption capacity play a primary role in enhancing microbial growth while also contributing to bacterial attachment. However, despite these insights, more detailed research is needed to fully understand the specific physical and chemical interactions between filamentous algae and biochar-enhanced mortar, such as identifying the role of surface functional groups in biochar–algal interactions., which remains an important area for further investigation.

Comparing the two species, *Scenedesmus* sp. consistently outperformed *Chlorella* sp., mirroring results observed during flask cultivation (Figure 7a,b). This is likely due to *Scenedesmus* sp.'s physiological traits, which make it more efficient at utilizing $CO_2$ and adapting to a broader range of environmental conditions [64]. Its adaptability enables *Scenedesmus* sp. to take greater advantage of the increased surface area and nutrient availability in biochar-enhanced environments. Additionally, *Scenedesmus* sp.'s superior ability to retain nutrients and efficiently sequester $CO_2$ likely contributed to its stronger growth response [62], particularly at higher biochar concentrations, such as CSB50 and CSB75. These combined factors allowed *Scenedesmus* sp. to achieve greater biomass accumulation, demonstrating its enhanced capacity to thrive in biochar-enriched environments compared with *Chlorella* sp.

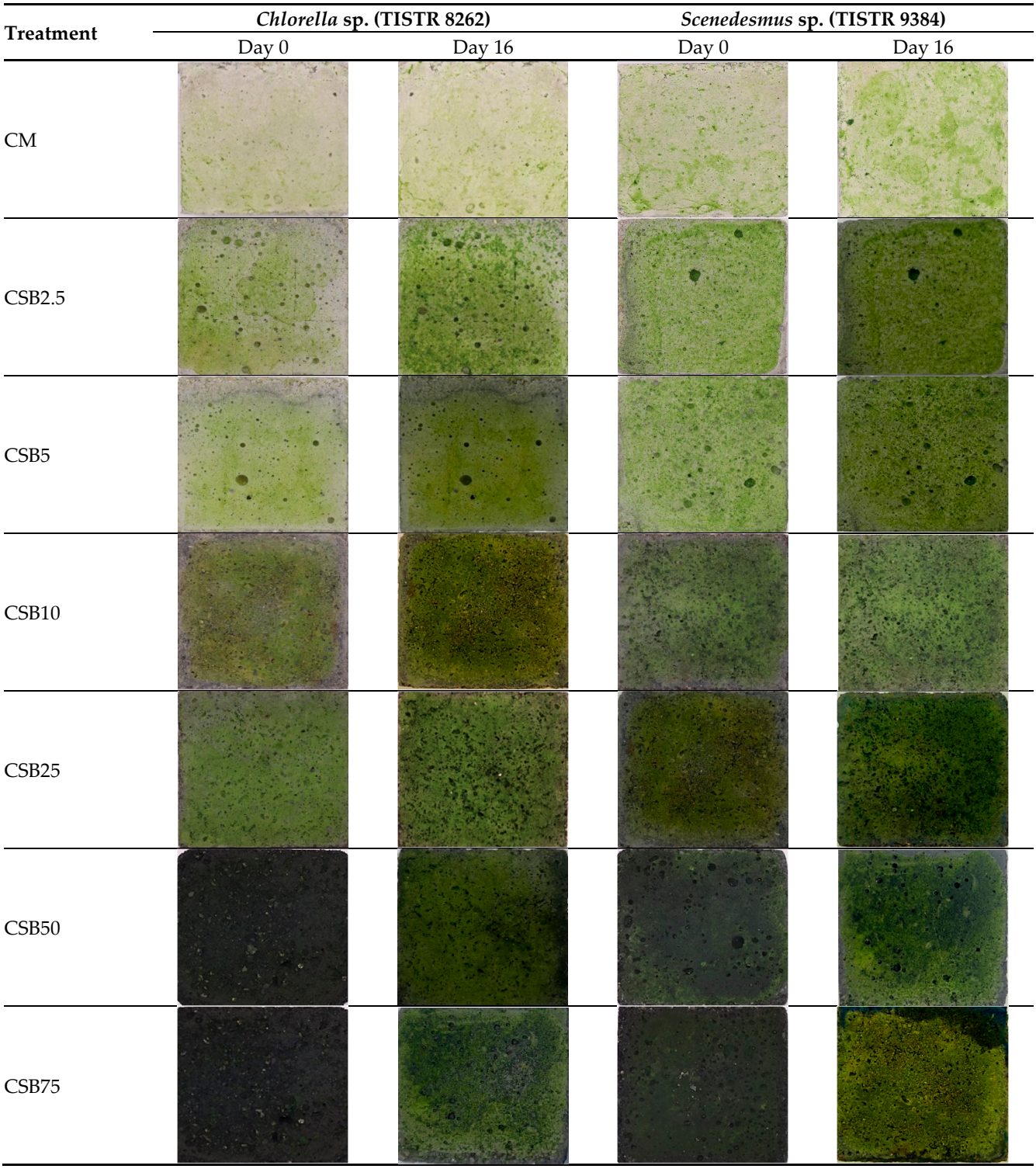



**Figure 8.** Visual comparison of *Chlorella* sp. (TISTR 8262) and *Scenedesmus* sp. (TISTR 9384) growth on corn stalk biochar (CSB)-enhanced mortar between day 0 and day 16.

Nevertheless, the reduction in both algae on CSB-enhanced mortars, particularly at higher concentrations like CSB50 and CSB75 after day 12, can be attributed to several factors leading to their earlier transition into the stationary phase. One possible explanation is that the high biochar content may adsorb metabolites, introducing environmental stress in the growth medium and creating competition for nutrients. As Hill et al. [79] suggested, such stressors can significantly impact microbial growth, which may alter the balance of the microbial community. Additionally, the production of EPS may be inhibited at

these elevated biochar concentrations due to changes in surface roughness and nutrient availability. These alterations can disrupt the optimal conditions required for continuous growth, particularly after day 12, hindering sustained algal proliferation and causing both species to experience a decline.

#### 3.4.2. Carbon Dioxide Absorption

The variations in $CO_2$ absorption ratios across CSB-enhanced mortar demonstrate the positive impact of biochar on $CO_2$ sequestration efficiency (Figure 9a). In the CM sample, the $CO_2$ absorption ratio (expressed as a percentage) began at 19.7% on day 0 and gradually increased to 48.1% by day 6, remaining constant through day 16, indicating limited sequestration capacity. However, the introduction of low levels of CSB (CSB2.5) resulted in a notable improvement, with the ratio starting at 20.8% on day 0 and reaching 52.3% by day 16, a 9% increase over the control. As biochar concentration increased, $CO_2$ absorption efficiency continued to improve, with CSB10 reaching 66.7% (a 39% increase), CSB25 reaching 71.8% (a 50% increase), and CSB50 peaking at 78.8% (a 64% improvement). The highest concentration, CSB75, achieved the greatest absorption ratio of 86.0%, marking a 79% increase over the control.

These results reinforce the well-established role of biochar as an effective medium for enhancing carbon sequestration. As biochar concentration increased, so did the absorption efficiency, primarily due to the larger surface area and greater porosity of the mortar, which allowed more $CO_2$ to be captured. The $CO_2$ adsorption capacity of biochar, as demonstrated by the BET results in Figure 4a, is influenced by various physicochemical properties. Zhang et al. [85] explained that $CO_2$ adsorption on biochar surfaces occurs through van der Waals forces between gas molecules and the solid phase, which are strongly associated with the specific surface area, pore size, and pore volume of the biochar. A larger surface area, combined with increased pore volume, provides more active sites for the physical adsorption of $CO_2$, resulting in a greater overall adsorption capacity [86,87].

Furthermore, the $CO_2$ absorption capacity of CSB, measured at 2.9 mmol $g^{-1}$ (Table 3), is largely influenced by its chemical properties, including surface functional groups, alkalinity, and mineral content. Key functional groups, such as hydroxyl (O–H), carboxyl, and carbonyl (C=O), identified through FTIR analysis (Figure 4), enhance $CO_2$ adsorption by facilitating hydrogen bonding between $CO_2$ molecules and the biochar surface [88]. Additionally, the presence of aromatic structures (C=C bonds) contributes to the stability of $CO_2$ retention, preventing rapid desorption and supporting long-term sequestration. This stability, along with biochar's hydrophobicity and non-polarity, further enhances its capacity to capture and retain $CO_2$ effectively over time [6]. Though the presence of alkali metals (e.g., Na, K, Ca, Mg, and Li) in biochar can promote the formation of basic sites with a strong affinity for CO2 [6,89], this might not be the case in this study. While these metals are likely present in the unwashed biochar due to residual ash, the pH values in the experiments were not particularly alkaline. The observed increase from 7 to 8 was more likely attributable to photosynthetic processes rather than the presence of alkali metals. It should be also noted that $CO_2$ adsorption capacity may be reduced in humid environments due to the high affinity of porous materials for water molecules [90,91]. Biochar with hydrophobic and non-polar characteristics could mitigate this issue by limiting the competition from water molecules, thereby maintaining or even enhancing its $CO_2$ adsorption capacity.

The observation that all treatments reached their peak $CO_2$ absorption by day 6 suggests that the mortar's $CO_2$ sequestration capacity had reached saturation. Once the biochar's surface area and pores became fully occupied by $CO_2$, further absorption was restricted, leading to the plateau in absorption across all treatments. This aligns with the findings of Gupta et al. [92], who also noted a saturation effect in similar systems. This

indicates that the $CO_2$ absorption potential is determined not only by the concentration of biochar but also by the physical and chemical limitations of the mortar matrix, which, once saturated, restricts further $CO_2$ uptake.

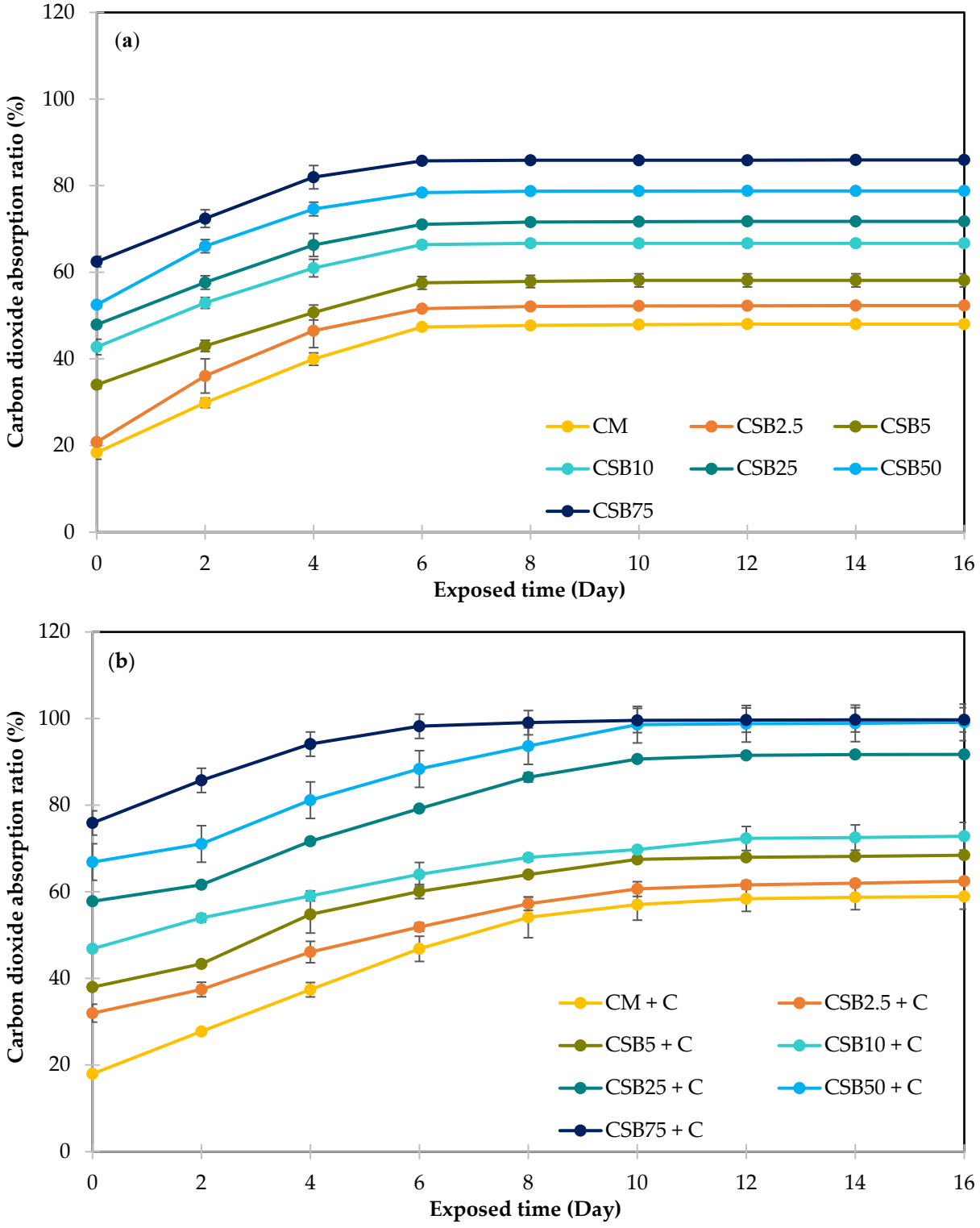



**Figure 9.** *Cont.*

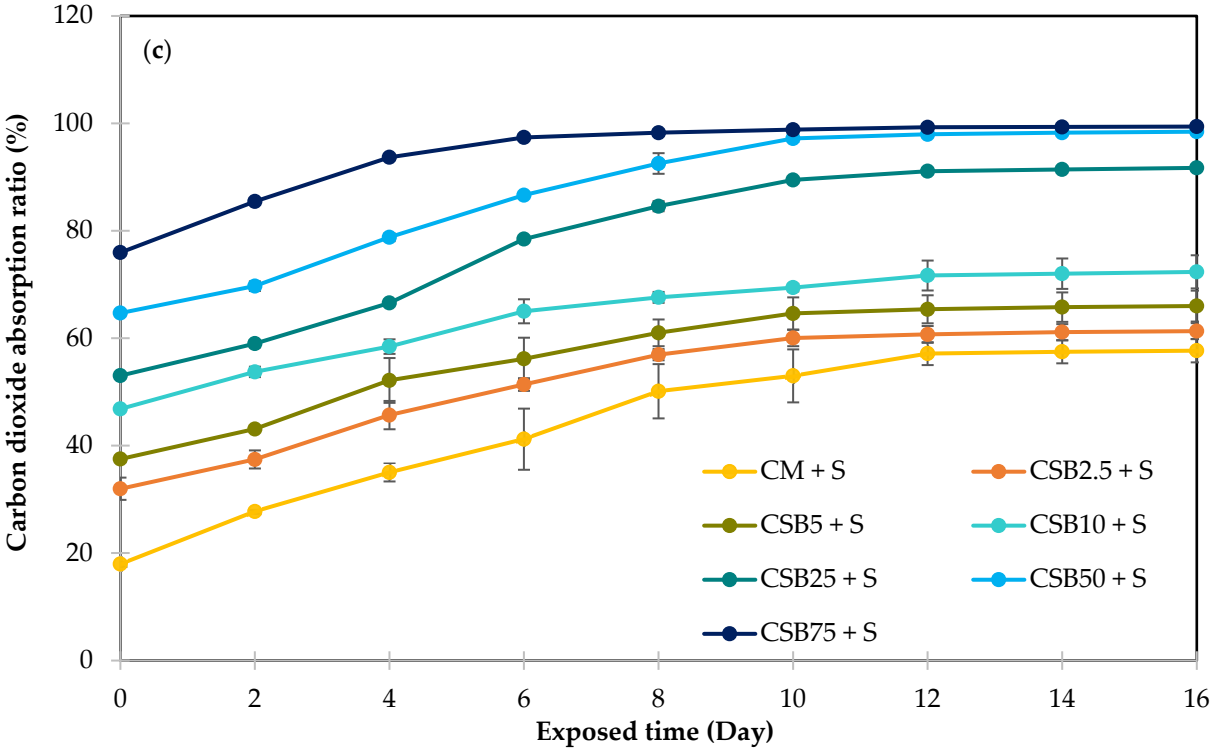



**Figure 9.** Variations in carbon dioxide ($CO_2$) absorption ratio of corn stalk biochar (CSB)-enhanced mortar at different concentrations (**a**), with *Chlorella* sp. (TISTR 8262) (**b**) and *Scenedesmus* sp. (TISTR 9384) (**c**) grown on the mortar surfaces.

The changes in $CO_2$ absorption ratios of CSB-enhanced mortar at varying concentrations, with *Chlorella* sp. and *Scenedesmus* sp. grown on the mortar surfaces, are presented in Figure 9b,c. The presence of algae significantly ($p < 0.05$) enhanced $CO_2$ absorption, with CSB-enhanced mortars containing algae exhibiting higher $CO_2$ sequestration compared with those without algae. Across both species, higher CSB concentrations consistently led to greater $CO_2$ absorption. For *Chlorella* sp., in the control condition (CM + C), the $CO_2$ absorption ratio started at 18.0% on day 0, gradually increasing to 58.7% by day 16. At lower concentrations of biochar (CSB2.5 and CSB5), the $CO_2$ absorption ratios peaked at around 61.6% and 68.0% by day 12, reflecting moderate growth in absorption efficiency. However, at higher concentrations such as CSB25, CSB50, and CSB75, the $CO_2$ absorption ratios nearly reached saturation, with values of 99.5%, 99.9%, and 99.9%, respectively, by day 16. This represents a significant enhancement in $CO_2$ absorption, with *Chlorella* sp. achieving nearly 100% efficiency at these higher biochar levels.

Similarly, *Scenedesmus* sp. followed a comparable trend, with the control condition (CM + S) starting at 17.9% and increasing to 57.7% by day 16 (Figure 9b,c). At lower biochar concentrations (CSB2.5 and CSB5), *Scenedesmus* sp. displayed absorption ratios of 61.3% and 64.6% by day 12, similar to *Chlorella* sp. However, at higher concentrations (CSB25, CSB50, and CSB75), the absorption ratios again approached complete $CO_2$ absorption, peaking at 99.4% by day 14 for CSB25 + S and reaching 99.5% and 99.9% by day 16 for CSB50 and CSB75, respectively. This shows that both algae species were highly efficient at $CO_2$ absorption when enhanced by higher biochar concentrations.

It is evident that the $CO_2$ absorption ratio stabilized more rapidly at higher concentrations of CSB. For instance, in both *Chlorella* sp. and *Scenedesmus* sp. experiments, the $CO_2$ absorption ratio for CSB75 reached a plateau as early as day 8. This rapid stabilization indicates that higher concentrations of biochar enhance the mortar's capacity to absorb $CO_2$ more efficiently. In comparison, lower concentrations of biochar, such as CSB2.5 and

CSB5, exhibited a more gradual increase in $CO_2$ absorption, stabilizing closer to day 12. This suggests that higher CSB levels not only increase $CO_2$ absorption but also lead to faster stabilization in the absorption process.

These findings highlight the significant role that biochar plays in enhancing $CO_2$ absorption capacity in mortar, particularly when combined with algae such as *Chlorella* sp. and *Scenedesmus* sp. The presence of algae dramatically increased $CO_2$ sequestration efficiency due to their photosynthetic activity, which utilizes $CO_2$ as a key substrate for producing oxygen and carbohydrates [93,94]. As biochar concentrations increased, mortars were able to absorb more $CO_2$, creating favorable conditions for algae growth and more efficient photosynthesis. Additionally, the faster stabilization of $CO_2$ absorption at higher biochar concentrations suggests that biochar improved both the physical absorption of $CO_2$ by the mortar and the biological uptake by the algae, allowing the system to reach saturation more quickly. This synergistic relationship between biochar and algae underscores the effectiveness of combining these two components for significantly enhanced $CO_2$ sequestration in mortar, providing a promising strategy for improving carbon capture in practical applications.

When comparing the two species, *Scenedesmus* sp. marginally outperformed *Chlorella* sp. at the highest biochar concentrations, demonstrating a faster increase in absorption ratios and reaching its peak slightly earlier (Figure 9b,c). For example, *Scenedesmus* sp. reached its maximum absorption ratio by day 14 at CSB25 and maintained a consistent advantage over *Chlorella* sp. at higher biochar concentrations, such as CSB50 and CSB75. The slight advantage observed for *Scenedesmus* sp. over *Chlorella* sp. in $CO_2$ absorption at higher biochar concentrations can be attributed to the physiological and adaptive differences between the two species. *Scenedesmus* sp. may have a greater tolerance for the increased surface area and porosity provided by higher biochar levels, allowing it to more effectively utilize $CO_2$ for photosynthesis. A study by Li et al. [93] demonstrated that the $CO_2$ fixation potential of *Scenedesmus* sp. is species-specific, with this species exhibiting superior performance compared with *Chlorella sorokiniana* GS03 and *Chlorella pyrenoidosa* SJTU-2 under similar conditions.

Interestingly, the faster rise in $CO_2$ absorption ratios and earlier stabilization seen in *Scenedesmus* sp. suggests that it is better suited for environments with higher biochar content. These conditions may create a more favorable environment for its growth and $CO_2$ sequestration. This efficiency at higher biochar concentrations indicates that *Scenedesmus* sp. could be more effective in systems where maximum $CO_2$ absorption is required in a shorter time frame, making it a potentially advantageous species for biochar-enhanced carbon capture applications.

In practical applications, the concentration of CSB in cement mortar must be carefully adjusted to balance structural integrity, carbon sequestration potential, and practical concerns such as water absorption. The primary objective of this research is to explore the use of biochar-enhanced cement mortar as a dual-purpose material—both as a construction medium and as a platform for algae cultivation to enhance carbon capture. This approach aims to contribute not only to the strength of the material but also to its environmental sustainability.

For structural applications, where load-bearing is crucial (e.g., foundations, beams, or columns), lower CSB concentrations (up to 5%) are recommended. This ensures modest $CO_2$ absorption without compromising the mortar's strength and durability. This provides an innovative solution by enabling the material to capture carbon while maintaining its structural integrity for load-bearing applications. These materials can be used in building designs that prioritize both environmental benefits and strength. In non-structural applications, such as facades, decorative elements, or paving stones, moderate CSB concentrations (10–25%) offer a balance between adequate strength and enhanced $CO_2$ sequestration.

These applications can tolerate a slight reduction in strength in exchange for significant environmental benefits, specifically increased $CO_2$ removal through algae photosynthesis. This makes the material ideal for green infrastructure applications, where reducing environmental impact is prioritized over structural performance.

For bioactive facades and other green infrastructure applications, higher CSB concentrations (50–75%) can be used to maximize $CO_2$ capture. These concentrations are particularly suited for bioactive building surfaces designed to support algae growth for carbon capture or bioremediation. Such applications are especially relevant in urban areas, where bioactive surfaces can play a significant role in sustainability efforts by reducing $CO_2$ levels in the atmosphere and promoting biodiversity.

However, a key consideration is that both algae and high biochar concentrations can increase water retention in the substrate, potentially leading to issues such as excessive moisture and reduced energy efficiency due to compromised insulation. Additionally, high biochar content reduces the compressive strength and density of the mortar. To address the challenge of low compressive strength in high-CSB mortars, hybrid material systems could be explored. These systems could combine biochar with other strengthening agents or reinforcement strategies, such as fibers or polymers, to improve the mortar's load-bearing capacity while maintaining its $CO_2$ sequestration ability. Moreover, reinforcement with materials like steel mesh or carbon fibers could enhance the structural performance of biochar-enhanced mortars, making them more suitable for applications that require load-bearing capacity. These approaches could enable the use of high-CSB mortars in applications that benefit from their carbon-negative properties while also addressing strength limitations.

Therefore, while these formulations show promise for carbon-negative construction and eco-friendly landscaping, they should be limited to non-load-bearing applications. These materials should be designed to manage water retention, structural integrity, and energy efficiency effectively. In this way, they can be optimized for use in non-load-bearing applications such as landscaping, bioactive facades, and decorative elements, where sustainability and environmental impact reduction are the primary goals.

## 4. Conclusions

This study highlights the novel potential of incorporating CSB into cement mortar, particularly for enhancing carbon sequestration and supporting algae growth. The unique physicochemical properties of CSB, including its high carbon content, porosity, and large surface area, make it an ideal candidate for dual-purpose applications that improve both structural performance and environmental sustainability. The incorporation of biochar significantly increased the mortar's $CO_2$ absorption capacity, with concentrations above 25% showing the most notable improvements. At the highest CSB concentration of 75%, the mortar without algae achieved a $CO_2$ absorption ratio of 86%, while the inclusion of algae increased this ratio to nearly 100%, highlighting the synergistic effect between biochar and algal photosynthesis. Among the two species studied, *Scenedesmus* sp. outperformed *Chlorella* sp. in $CO_2$ absorption, particularly at higher biochar concentrations. This is likely due to *Scenedesmus*'s greater adaptability to the biochar's porous structure and increased surface area.

Looking forward, several areas of future research are critical to optimize the use of biochar-enhanced mortar. Long-term durability studies are essential to assess the performance and sustainability of CSB-enhanced mortars, especially in real-world conditions, including exposure to weathering, mechanical stress, and the potential for $CO_2$ saturation over time. Such studies will be crucial in determining the long-term viability of these

materials for infrastructure applications, ensuring that their environmental benefits do not come at the expense of performance.

Hybrid systems that combine algae with other complementary carbon capture technologies may extend the $CO_2$ absorption capacity of these materials in the long term. Additionally, exploring other biomass sources for biochar production could provide materials with specific characteristics better suited to enhancing both the structural integrity and carbon capture efficiency of the mortar. Scaling up the findings from this study to pilot-scale projects would provide valuable insights into the feasibility of using biochar-enhanced mortar in large-scale construction. Lastly, conducting a life cycle analysis of biochar-enhanced mortar systems will offer a comprehensive view of their environmental impact, including the carbon footprint of biochar production, transportation, and use. Economic assessments, including cost–benefit analysis, will be crucial in determining the long-term financial viability of biochar-enhanced mortar as a sustainable, carbon-negative construction material for the future.

**Author Contributions:** Conceptualization, P.K.; designing and conducting the experiment, S.S. and A.J.; data curation, P.U.; writing—original draft preparation, S.S. and P.U.; writing—review and editing, K.K., M.G. and P.K.; supervision, P.K. All authors have read and agreed to the published version of the manuscript.

**Funding:** This review was financially supported by the Fundamental Fund, Chiang Mai University, the NSRF via the Program Management Unit for Human Resources & Institutional Development, Research, and Innovation (grant number B40G660030), and partially by Chiang Mai University.

**Institutional Review Board Statement:** Not applicable.

**Informed Consent Statement:** Not applicable.

**Data Availability Statement:** Data are contained within the article.

**Acknowledgments:** This research was generously supported by Chiang Mai University and Prince of Songkla University.

**Conflicts of Interest:** The authors declare no conflicts of interest.

## References

1. Marescaux, A.; Thieu, V.; Garnier, J. Carbon dioxide, methane, and nitrous oxide emissions from the human-impacted Seine watershed in France. *Sci. Total Environ.* **2018**, *643*, 247–259. [CrossRef] [PubMed]
2. IPCC. *Climate Change 2013: The Physical Science Basis. Contribution of Working Group I to the Fifth Assessment Report of the Intergovernmental Panel on Climate Change*; Cambridge University Press: Cambridge, UK; New York, NY, USA, 2013; p. 1535. Available online: https://ipcc.ch/site/assets/uploads/2018/02/WG1AR5_all_final.pdf (accessed on 30 September 2024).
3. Filonchyk, M.; Peterson, M.P.; Zhang, L.; Hurynovich, V.; He, Y. Greenhouse gases emissions and global climate change: Examining the influence of $CO_2$, $CH_4$, and $N_2O$. *Sci. Total Environ.* **2024**, *935*, 173359. [CrossRef]
4. Weiskopf, S.R.; Rubenstein, M.A.; Crozier, L.G.; Gaichas, S.; Griffis, R.; Halofsky, J.E.; Hyde, K.J.W.; Morelli, T.L.; Morisette, J.T.; Muñoz, R.C.; et al. Climate change effects on biodiversity, ecosystems, ecosystem services, and natural resource management in the United States. *Sci. Total Environ.* **2020**, *733*, 137782. [CrossRef] [PubMed]
5. Zhang, X.; Gao, B.; Creamer, A.E.; Cao, C.; Li, Y. Adsorption of VOCs onto engineered carbon materials: A review. *J. Hazard. Mater.* **2017**, *338*, 102–123. [CrossRef] [PubMed]
6. Dissanayake, P.D.; You, S.; Igalavithana, A.D.; Xia, Y.; Bhatnagar, A.; Gupta, S.; Kua, H.W.; Kim, S.; Kwon, J.H.; Tsang, D.C.W.; et al. Biochar-based adsorbents for carbon dioxide capture: A critical review. *Renew. Sustain. Energy Rev.* **2020**, *119*, 109582. [CrossRef]
7. Ahmad, M.; Lee, S.S.; Lee, S.E.; Al-Wabel, M.I.; Tsang, D.C.W.; Ok, Y.S. Biochar-induced changes in soil properties affected immobilization/mobilization of metals/metalloids in contaminated soils. *J. Soils Sediments* **2017**, *17*, 717–730. [CrossRef]
8. Beiyuan, J.; Awad, Y.M.; Beckers, F.; Tsang, D.C.W.; Ok, Y.S.; Rinklebe, J. Mobility and phytoavailability of As and Pb in a contaminated soil using pine sawdust biochar under systematic change of redox conditions. *Chemosphere* **2017**, *178*, 110–118. [CrossRef]

9. El-Naggar, A.; Lee, S.S.; Awad, Y.M.; Yang, X.; Ryu, C.; Rizwan, M.; Rinklebe, J.; Tsang, D.C.W.; Ok, Y.S. Influence of soil properties and feedstocks on biochar potential for carbon mineralization and improvement of infertile soils. *Geoderma* **2018**, *332*, 100–108. [CrossRef]
10. Gong, Y.; Hou, R.; Fu, Q.; Li, T.; Wang, J.; Su, Z.; Shen, W.; Zhou, W.; Wang, Y.; Li, M. Modified biochar reduces the greenhouse gas emission intensity and enhances the net ecosystem economic budget in black soil soybean fields. *Soil Tillage Res.* **2024**, *237*, 105978. [CrossRef]
11. Li, Y.; Ruan, G.; Jalilov, A.S.; Tarkunde, Y.R.; Fei, H.; Tour, J.M. Biochar as a renewable source for high-performance $CO_2$ sorbent. *Carbon* **2016**, *107*, 344–351. [CrossRef]
12. Huang, H.; Tang, J.; Gao, K.; He, R.; Zhao, H.; Werner, D. Characterization of KOH modified biochars from different pyrolysis temperatures and enhanced adsorption of antibiotics. *RSC Adv.* **2017**, *7*, 14640–14648. [CrossRef]
13. Churkina, G.; Organschi, A.; Reyer, C.P.O.; Ruff, A.; Vinke, K.; Liu, Z.; Reck, B.K.; Graedel, T.E.; Schellnhuber, H.J. Buildings as a global carbon sink. *Nat. Sustain.* **2020**, *3*, 269–276. [CrossRef]
14. Praneeth, S.; Saavedra, L.; Zeng, M.; Dubey, B.K.; Sarmah, A.K. Biochar admixtured lightweight, porous and tougher cement mortars: Mechanical, durability and micro computed tomography analysis. *Sci. Total Environ.* **2021**, *750*, 142327. [CrossRef]
15. Suarez-Riera, D.; Restuccia, L.; Ferro, G.A. The use of Biochar to reduce the carbon footprint of cement-based materials. *Procedia Struct. Integr.* **2020**, *26*, 199–210. [CrossRef]
16. Song, S.; Liu, Z.; Liu, G.; Cui, X.; Sun, J. Application of biochar cement-based materials for carbon sequestration. *Constr. Build. Mater.* **2023**, *405*, 133373. [CrossRef]
17. Mrad, R.; Chehab, G. Mechanical and microstructure properties of biochar-based mortar: An internal curing agent for PCC. *Sustainability* **2019**, *11*, 2491. [CrossRef]
18. Aziz, M.A.; Zubair, M.; Saleem, M.; Alharthi, Y.M.; Ashraf, N.; Alotaibi, K.S.; Aga, O.; Al Eid, A.A.A. Mechanical, non-destructive, and thermal characterization of biochar-based mortar composite. *Biomass Convers. Biorefinery* **2023**. [CrossRef]
19. Room, S.; Bahadori-Jahromi, A. Biochar-enhanced carbon-negative and sustainable cement composites: A scientometric review. *Sustainability* **2024**, *16*, 10162. [CrossRef]
20. Rupasinghe, M.; Zhang, Z.; Mendis, P.; Sofi, M. Carbon sequestering biochar incorporated cementitious composites: Evaluation of hygrothermal, mechanical and durability characteristics. *Cement Concr. Compos.* **2025**, *157*, 105864. [CrossRef]
21. Alum, A.; Rashid, A.; Mobasher, B.; Abbaszadegan, M. Cement-based biocide coatings for controlling algal growth in water distribution canals. *Cem. Concr. Compos.* **2008**, *30*, 839–847. [CrossRef]
22. Martinez, T.; Bertron, A.; Escadeillas, G.; Ringot, E. Algal growth inhibition on cement mortar: Efficiency of water repellent and photocatalytic treatments under UV/VIS illumination. *Int. Biodeterior. Biodegrad.* **2014**, *89*, 115–125. [CrossRef]
23. Alazaiza, M.Y.D.; Albahnasawi, A.; Eyvaz, M.; Al Maskari, T.; Nassani, D.E.; Abu Amr, S.S.; Abujazar, M.S.S.; Bashir, M.J.K. An overview of green bioprocessing of algae-derived biochar and biopolymers: Synthesis, preparation, and potential applications. *Energies* **2023**, *16*, 791. [CrossRef]
24. Wang, Y.; Ma, C.; Kong, D.; Lian, L.; Liu, Y. Review on application of algae-based biochars in environmental remediation: Progress, challenge, and perspectives. *J. Environ. Chem. Eng.* **2023**, *11*, 111263. [CrossRef]
25. Behl, K.; Sinha, S.; Sharma, M.; Singh, S.; Joshi, M.; Bhatnagar, A.; Nigam, S. One-time cultivation of *Chlorella pyrenoidosa* in aqueous dye solution supplemented with biochar for microalgal growth, dye decolorization, and lipid production. *Chem. Eng. J.* **2019**, *364*, 552–561. [CrossRef]
26. Ramos-Ibarra, J.R.; Snell-Castro, R.; Neria-Casillas, J.A.; Choix, F.J. Biotechnological potential of *Chlorella* sp. and *Scenedesmus* sp. microalgae to endure high $CO_2$ and methane concentrations from biogas. *Bioprocess Biosyst. Eng.* **2019**, *42*, 1603–1610. [CrossRef] [PubMed]
27. Nagi, M.; He, M.; Li, D.; Gebreluel, T.; Cheng, B.; Wang, C. Utilization of tannery wastewater for biofuel production: New insights on microalgae growth and biomass production. *Sci. Rep.* **2020**, *10*, 1530. [CrossRef] [PubMed]
28. Pandian, P.M.; Dharkshith, K.; Muthiah, P. Improvising biodiesel production from *Scenedesmus dimorphus* via nutrient starvation and optimized pretreatment process. *BioEnergy Res.* **2024**, *17*, 2400–2412. [CrossRef]
29. Gotore, O.; Rameshprabu, R.; Itayama, T. Adsorption performances of corn cob-derived biochar in saturated and semi-saturated vertical-flow constructed wetlands for nutrient removal under erratic oxygen supply. *Environ. Chem. Ecotoxicol.* **2022**, *4*, 155–163. [CrossRef]
30. *ASTM C33*; Standard Specification for Concrete Aggregates. ASTM International: Philadelphia, PA, USA, 2012.
31. *ASTM C109/C109M-20b*; Standard Test Method for Compressive Strength of Hydraulic Cement Mortars (Using 2-in. or [50 mm] Cube Specimens). ASTM International: Philadelphia, PA, USA, 2020.
32. *ASTM C305*; Standard Practice for Mechanical Mixing of Hydraulic Cement Pastes and Mortars of Plastic Consistency. ASTM International: Philadelphia, PA, USA, 2002.
33. *ASTM C188-17*; Standard Test Method for Density of Hydraulic Cement. ASTM International: Philadelphia, PA, USA, 2023.

34. *ASTM C1403-15*; Standard Test Method for Rate of Water Absorption of Masonry Mortars. ASTM International: Philadelphia, PA, USA, 2022.
35. Carneiro, M.; Ranglová, K.; Lakatos, G.E.; Manoel, J.A.C.; Grivalský, T.; Kozhan, D.M.; Toribio, A.; Moreno, G.; Otero, A.; Varela, J.; et al. Growth and bioactivity of two chlorophyte (*Chlorella* and *Scenedesmus*) strains co-cultured outdoors in two different thin-layer units using municipal wastewater as a nutrient source. *Algal Res.* **2021**, *56*, 102299. [CrossRef]
36. Wei, X.; Yu, G.; Cao, W.; Feng, M.; Xu, Y.; Jin, M.; Zhang, Y.; Li, T.; Guo, L. Biomass producing and $CO_2$ capturing simultaneously by *Chlorella vulgaris*: Effect of $CO_2$ concentration and aeration rate. *Energy* **2024**, *306*, 132321. [CrossRef]
37. Yin, D.; Wang, Z.; Wen, X.; Ding, Y.; Hou, X.; Geng, Y.; Li, Y. Effects of carbon concentration, pH, and bubbling depth on carbon dioxide absorption ratio in microalgae medium. *Environ. Sci. Pollut. Res.* **2019**, *26*, 32902–32910. [CrossRef] [PubMed]
38. Li, L.; Zhang, H.; Liu, Z.; Su, Y.; Du, C. Adsorbent biochar derived from corn stalk core for highly efficient removal of bisphenol A. *Environ. Sci. Pollut. Res.* **2023**, *30*, 74916–74927. [CrossRef]
39. Wang, L.; Olsen, M.N.P.; Moni, C.; Dieguez-Alonso, A.; de la Rosa, J.M.; Stenrød, M.; Liu, X.; Mao, L. Comparison of properties of biochar produced from different types of lignocellulosic biomass by slow pyrolysis at 600 °C. *Appl. Energy Combust. Sci.* **2022**, *12*, 100090. [CrossRef]
40. Yan, S.; Yu, W.; Yang, T.; Li, Q.; Guo, J. The adsorption of corn stalk biochar for Pb and Cd: Preparation, characterization, and batch adsorption study. *Separations* **2022**, *9*, 22. [CrossRef]
41. Karimi, M.; Shirzad, M.; Silva, J.A.C.; Rodrigues, A.E. Biomass/Biochar carbon materials for $CO_2$ capture and sequestration by cyclic adsorption processes: A review and prospects for future directions. *J. CO2 Util.* **2022**, *57*, 101890. [CrossRef]
42. Mamaghani, Z.G.; Hawboldt, K.A.; MacQuarrie, S. Adsorption of $CO_2$ using biochar—Review of the impact of gas mixtures and water on adsorption. *J. Environ. Chem. Eng.* **2023**, *11*, 109643. [CrossRef]
43. Ding, Y.; Liu, Y.; Liu, S.; Li, Z.; Tan, X.; Huang, X.; Zeng, G.; Zhou, Y.; Zheng, B.; Cai, X. Competitive removal of Cd(II) and Pb(II) by biochars produced from water hyacinths: Performance and mechanism. *RSC Adv.* **2016**, *6*, 5223–5232. [CrossRef]
44. Chen, X.; Chen, G.; Chen, L.; Chen, Y.; Lehmann, J.; McBride, M.B.; Hay, A.G. Adsorption of copper and zinc by biochars produced from pyrolysis of hardwood and corn straw in aqueous solution. *Bioresour. Technol.* **2011**, *102*, 8877–8884. [CrossRef]
45. Salehi, E.; Askari, M.; Velashjerdi, M.; Arab, B. Phosphoric acid-treated spent tea residue biochar for wastewater decoloring: Batch adsorption study and process intensification using multivariate data-based optimization. *Chem. Eng. Process Intensif.* **2020**, *158*, 108170. [CrossRef]
46. Tang, L.; Yang, G.-D.; Zeng, G.-M.; Cai, Y.; Li, S.-S.; Zhou, Y.; Pang, Y.; Liu, Y.-Y.; Zhang, Y.; Luna, B. Synergistic effect of iron doped ordered mesoporous carbon on adsorption-coupled reduction of hexavalent chromium and the relative mechanism study. *Chem. Eng. J.* **2014**, *239*, 114–122. [CrossRef]
47. Keiluweit, M.; Nico, P.S.; Johnson, M.G.; Kleber, M. Dynamic molecular structure of plant biomass-derived black carbon (biochar). *Environ. Sci. Technol.* **2010**, *44*, 1247–1253. [CrossRef] [PubMed]
48. Janu, R.; Mrlik, V.; Ribitsh, D.; Hofman, J.; Sedlacek, P.; Bielska, L.; Soja, G. Biochar surface functional groups as affected by biomass feedstock, biochar composition and pyrolysis temperature. *Carbon Resour. Convers.* **2021**, *4*, 36–46. [CrossRef]
49. Li, Q.; Yu, W.; Guo, L.; Wang, Y.; Zhao, S.; Zhou, L.; Jiang, X. Sorption of sulfamethoxazole on inorganic acid solution-etched biochar derived from alfalfa. *Materials* **2021**, *14*, 1033. [CrossRef] [PubMed]
50. Sahoo, S.S.; Vijay, V.K.; Chandra, R.; Kumar, H. Production and characterization of biochar produced from slow pyrolysis of pigeon pea stalk and bamboo. *Clean. Eng. Technol.* **2021**, *3*, 100101. [CrossRef]
51. Gupta, S.; Kua, H.W. Effect of water entrainment by pre-soaked biochar particles on strength and permeability of cement mortar. *Constr. Build. Mater.* **2018**, *159*, 107–125. [CrossRef]
52. Wang, L.; Chen, L.; Tsang, D.C.W.; Guo, B.; Yang, J.; Shen, Z.; Hou, D.; Ok, Y.S.; Poon, C.S. Biochar as green additives in cement-based composites with carbon dioxide curing. *J. Clean. Prod.* **2020**, *258*, 120678. [CrossRef]
53. Zhao, Z.; El-Naggar, A.; Kau, J.; Olson, C.; Tomlinson, D.; Chang, S.X. Biochar affects compressive strength of Portland cement composites: A meta-analysis. *Biochar* **2024**, *6*, 21. [CrossRef]
54. Liu, W.; Li, K.; Xu, S. Utilizing bamboo biochar in cement mortar as a bio-modifier to improve the compressive strength and crack-resistance fracture ability. *Constr. Build. Mater.* **2022**, *327*, 126917. [CrossRef]
55. Pan, S.Y.; Adhikari, R.; Chen, Y.H.; Li, P.; Chiang, P.C. Integrated and innovative steel slag utilization for iron reclamation, green material production and $CO_2$ fixation via accelerated carbonation. *J. Clean. Prod.* **2016**, *137*, 617–631. [CrossRef]
56. Jhatial, A.A.; Goh, W.I.; Mohamad, N.; Sohu, S.; Lakhiar, M.T. Utilization of palm oil fuel ash and eggshell powder as partial cement replacement-a review. *Civ. Eng. J.* **2018**, *4*, 1977–1984. [CrossRef]
57. Akhtar, A.; Sarmah, A.K. Novel biochar-concrete composites: Manufacturing, characterization and evaluation of the mechanical properties. *Sci. Total Environ.* **2018**, *616–617*, 408–416. [CrossRef]
58. Brewer, C.E.; Chuang, V.J.; Masiello, C.A.; Gonnermann, H.; Gao, X.; Dugan, B.; Driver, L.E.; Panzacchi, P.; Zygourakis, K.; Davies, C.A. New approaches to measuring biochar density and porosity. *Biomass Bioenergy* **2014**, *66*, 176–185. [CrossRef]

59. Cuthbertson, D.; Berardi, U.; Briens, C.; Berruti, F. Biochar from residual biomass as a concrete filler for improved thermal and acoustic properties. *Biomass Bioenergy* **2019**, *120*, 77–83. [CrossRef]
60. Zeidabadi, Z.A.; Bakhtiari, S.; Abbaslou, H.; Ghanizadeh, A.R. Synthesis, characterization and evaluation of biochar from agricultural waste biomass for use in building materials. *Constr. Build. Mater.* **2018**, *181*, 301–308. [CrossRef]
61. Akinyemi, B.A.; Adesina, A. Recent advancements in the use of biochar for cementitious applications: A review. *J. Build. Eng.* **2020**, *32*, 101705. [CrossRef]
62. Oukarroum, A. Change in photosystem II photochemistry during algal growth phases of *Chlorella vulgaris* and *Scenedesmus obliquus*. *Curr. Microbiol.* **2016**, *72*, 692–699. [CrossRef] [PubMed]
63. Falkowski, P.; Raven, J. *Aquatic Photosynthesis*, 2nd ed.; Princeton University Press: Princeton, NJ, USA, 2007. [CrossRef]
64. Zhang, C.; Ho, S.H.; Li, A.; Fu, L.; Zhou, D. Co-culture of *Chlorella* and *Scenedesmus* could enhance total lipid production under bacteria quorum sensing molecule stress. *J. Water Process Eng.* **2021**, *39*, 101739. [CrossRef]
65. Shaima, A.F.; Yasin, N.H.M.; Ibrahim, N.; Takriff, M.S.; Gunasekaran, D.; Ismaeel, M.Y.Y. Unveiling antimicrobial activity of microalgae *Chlorella sorokiniana* (UKM2), *Chlorella* sp. (UKM8) and *Scenedesmus* sp. (UKM9). *Saudi J. Biol. Sci.* **2022**, *29*, 1043–1052. [CrossRef] [PubMed]
66. Sabatini, S.E.; Juarez, A.B.; Eppis, M.R.; Bianchi, L.; Luquet, C.M.; Ríos de Molina, M.d.C. Oxidative stress and antioxidant defenses in two green microalgae exposed to copper. *Ecotoxicol. Environ. Saf.* **2009**, *72*, 1200–1206. [CrossRef]
67. Vonshak, A.; Torzillo, G. Chapter 4: Environmental stress physiology. In *Handbook of Microalgal Culture: Biotechnology and Applied Phycology*; Richmond, A., Ed.; Wiley-Blackwell: Oxford, UK, 2003. [CrossRef]
68. Gao, K.; Campbell, D.A. Photophysiological responses of marine diatoms to elevated $CO_2$ and decreased pH: A review. *Funct. Plant Biol.* **2014**, *41*, 449–459. [CrossRef]
69. Chiu, S.Y.; Kao, C.Y.; Chen, T.Y.; Chang, Y.B.; Kuo, C.M.; Lin, C.S. Cultivation of microalgal *Chlorella* for biomass and lipid production using wastewater as nutrient resource. *Bioresour. Technol.* **2015**, *184*, 179–189. [CrossRef] [PubMed]
70. Masojídek, J.; Torzillo, G.; Koblízek, M.; Kopecký, J.; Bernardini, P.; Sacchi, A.; Komenda, J. Photoadaptation of two members of the *Chlorophyta* (*Scenedesmus* and *Chlorella*) in laboratory and outdoor cultures: Changes in chlorophyll fluorescence quenching and the xanthophyll cycle. *Planta* **1999**, *209*, 126–135. [CrossRef]
71. Lacour, T.; Babin, M.; Lavaud, J. Diversity in xanthophyll cycle pigments content and related nonphotochemical quenching (NPQ) among microalgae: Implications for growth strategy and ecology. *J. Phycol.* **2020**, *56*, 245–263. [CrossRef] [PubMed]
72. Lemoine, Y.; Schoefs, B. Secondary ketocarotenoid astaxanthin biosynthesis in algae: A multifunctional response to stress. *Photosynth. Res.* **2010**, *106*, 155–177. [CrossRef]
73. Ho, S.H.; Chen, C.Y.; Chang, J.S. Effect of light intensity and nitrogen starvation on $CO_2$ fixation and lipid/carbohydrate production of an indigenous microalga *Scenedesmus obliquus* CNW-N. *Bioresour. Technol.* **2012**, *113*, 244–252. [CrossRef]
74. Salama, E.S.; Kurade, M.B.; Abou-Shanab, R.A.I.; El-Dalatony, M.M.; Yang, I.S.; Min, B.; Jeon, B.H. Recent progress in microalgal biomass production coupled with wastewater treatment for biofuel generation. *Renew. Sustain. Energy Rev.* **2017**, *79*, 1189–1211. [CrossRef]
75. Giovannacci, D.; Leclaire, C.; Horgnies, M.; Ellmer, M.; Mertz, J.D.; Orial, G.; Chen, J.; Bousta, F. Algal colonization kinetics on roofing and façade tiles: Influence of physical parameters. *Constr. Build. Mater.* **2013**, *48*, 670–676. [CrossRef]
76. Tran, T.H.; Govin, A.; Guyonnet, R.; Grosseau, P.; Lors, C.; Damidot, D.; Deves, O.; Ruot, B. Influence of the intrinsic characteristics of mortars on their biofouling by pigmented organisms: Comparison between laboratory and field-scale experiments. *Int. Biodeterior. Biodegrad.* **2014**, *86*, 334–342. [CrossRef]
77. Tran, T.H.; Govin, A.; Guyonnet, R.; Grosseau, P.; Lors, C.; Damidot, D.; Devès, O.; Ruot, B. Avrami's law based kinetic modeling of colonization of mortar surface by alga *Klebsormidium flaccidum*. *Int. Biodeterior. Biodegrad.* **2013**, *79*, 73–80. [CrossRef]
78. Bolan, N.S.; Hou, D.; Wang, L.; Hale, L.; Egamberdieva, D.; Tammeorg, P.; Li, R.; Wang, B.; Xu, J.; Wang, T.; et al. The potential of biochar as a microbial carrier for agricultural and environmental applications. *Sci. Total Environ.* **2023**, *886*, 163968. [CrossRef] [PubMed]
79. Hill, R.A.; Hunt, J.; Sanders, E.; Tran, M.; Burk, G.A.; Mlsna, T.E.; Fitzkee, N.C. Effect of biochar on microbial growth: A metabolomics and bacteriological investigation in *E. coli*. *Environ. Sci. Technol.* **2019**, *53*, 2635–2646. [CrossRef]
80. Kholssi, R.; Marks, E.A.N.; Montero, O.; Maté, A.P.; Debdoubi, A.; Rad, C. The growth of filamentous microalgae is increased on biochar solid supports. *Biocatal. Agric. Biotechnol.* **2018**, *13*, 182–185. [CrossRef]
81. Shen, Y.; Li, H.; Zhu, W.; Ho, S.H.; Yuan, W.; Chen, J.; Xie, Y. Microalgal-biochar immobilized complex: A novel efficient biosorbent for cadmium removal from aqueous solution. *Bioresour. Technol.* **2017**, *244*, 1031–1038. [CrossRef]
82. Fang, Q.; Chen, B.; Lin, Y.; Guan, Y. Aromatic and hydrophobic surfaces of wood-derived biochar enhance perchlorate adsorption via hydrogen bonding to oxygen-containing organic groups. *Environ. Sci. Technol.* **2014**, *48*, 279–288. [CrossRef]
83. Mukherjee, A.; Zimmerman, A.R.; Harris, W. Surface chemistry variations among a series of laboratory-produced biochars. *Geoderma* **2011**, *163*, 247–255. [CrossRef]

84. Rivera-Utrilla, J.; Bautista-Toledo, I.; Ferro-García, M.A.; Moreno-Castilla, C. Activated carbon surface modifications by adsorption of bacteria and their effect on aqueous lead adsorption. *J. Chem. Technol. Biotechnol.* **2001**, *76*, 1209–1215. [CrossRef]
85. Zhang, X.; Zhang, S.; Yang, H.; Feng, Y.; Chen, Y.; Wang, X.; Chen, H. Nitrogen enriched biochar modified by high temperature $CO_2$–ammonia treatment: Characterization and adsorption of $CO_2$. *Chem. Eng. J.* **2014**, *257*, 20–27. [CrossRef]
86. Creamer, A.E.; Gao, B. Carbon-based adsorbents for postcombustion $CO_2$ capture: A critical review. *Environ. Sci. Technol.* **2016**, *50*, 7276–7289. [CrossRef] [PubMed]
87. You, S.; Ok, Y.S.; Chen, S.S.; Tsang, D.C.W.; Kwon, E.E.; Lee, J.; Wang, C.H. A critical review on sustainable biochar system through gasification: Energy and environmental applications. *Bioresour. Technol.* **2017**, *246*, 242–253. [CrossRef]
88. Liu, Y.; Wilcox, J. Effects of surface heterogeneity on the adsorption of $CO_2$ in microporous carbons. *Environ. Sci. Technol.* **2012**, *46*, 1940–1947. [CrossRef] [PubMed]
89. Xu, X.; Kan, Y.; Zhao, L.; Cao, X. Chemical transformation of $CO_2$ during its capture by waste biomass derived biochars. *Environ. Pollut.* **2016**, *213*, 533–540. [CrossRef]
90. Gao, F.; Li, Y.; Bian, Z.; Hu, J.; Liu, H. Dynamic hydrophobic hindrance effect of zeolite@zeolitic imidazolate framework composites for $CO_2$ capture in the presence of water. *J. Mater. Chem. A* **2015**, *3*, 8091–8097. [CrossRef]
91. Nugent, P.; Belmabkhout, Y.; Burd, S.D.; Elemento, O.; Giannopoulou, E.G.; Forrest, K.; Pham, T.; Ma, S.; Space, B.; Wojtas, L.; et al. Porous materials with optimal adsorption thermodynamics and kinetics for $CO_2$ separation. *Nature* **2013**, *495*, 80–84. [CrossRef]
92. Gupta, S.; Kua, H.W.; Low, C.Y. Use of biochar as carbon sequestering additive in cement mortar. *Cem. Concr. Compos.* **2018**, *87*, 110–129. [CrossRef]
93. Li, J.; Zhao, X.; Chang, J.S.; Miao, X. A two-stage culture strategy for *Scenedesmus* sp. FSP3 for $CO_2$ fixation and the simultaneous production of lutein under light and salt stress. *Molecules* **2022**, *27*, 7497. [CrossRef]
94. Yu, Q.; Wang, H.; Li, X.; Yin, Y.; Qin, S.; Ge, B. Enhanced biomass and $CO_2$ sequestration of *Chlorella vulgaris* using a new mixotrophic cultivation method. *Process Biochem.* **2020**, *90*, 168–176. [CrossRef]


**Disclaimer/Publisher's Note:** The statements, opinions and data contained in all publications are solely those of the individual author(s) and contributor(s) and not of MDPI and/or the editor(s). MDPI and/or the editor(s) disclaim responsibility for any injury to people or property resulting from any ideas, methods, instructions or products referred to in the content.